SOFTWARE TOOL FOR PERFORMING THE CALIBRATION OF THE AT-TPC ELECTRONICS CHANNELS

By

FELIX NDAYISABYE

A THESIS

Submitted to
Michigan State University
in partial fulfillment of the requirements
for the degree of

Physics-Master of Science

2019

ABSTRACT

SOFTWARE TOOL FOR PERFORMING THE CALIBRATION OF THE AT-TPC ELECTRONICS CHANNELS

By

FELIX NDAYISABYE

The Active Target Time Projection Chamber (AT-TPC), developed at the National Superconducting Cyclotron Laboratory (NSCL) at Michigan State University, is a gas-based system that serves a dual role of a target and detector medium for nuclear physics experiments. Active target devices have gained much attention within the past dedicate due to their high resolution and efficiency to study reactions with very exotic nuclei. With the use of incident beam energy ranging from low (1-10 MeV/u) to medium (10-100 MeV/u) to extract the physical properties of nuclei far from stability, the AT-TPC is contributing significantly to experimental nuclear science, thanks to its high luminosity working capability without loss of resolution and low-energy detection thresholds that enable experiments with beam intensities as low as 10^2 pps. Because of its unique features, a dedicated python based data analysis tool was developed to extract information from this detector. This software tool allows to calibrate the electronic baselines, amplitudes and times of the signals recorded by each of the AT-TPC pads relative to each other. The statistical analysis of the aforementioned calibrated parameters shows the coefficient of the fluctuations of the order of 9.1 % and 8.8 % for the baselines , 3.43 % and 4.8 % for the amplitudes and 45 **ns** and 34 **ns** for the time from the big and small pads respectively from all 24 events taken during the pulse run.

ACKNOWLEDGMENTS

First of all, I give thanks to the Lord God Almighty for giving me good health for the entire period of this studies. Graduate school has presented me with many of the most challenging and rewarding experiences of my life so far, and I owe an enormous debt of gratitude to everyone who helped me navigate this period of my life. I would like to express my great appreciation to my advisor Daniel Bazin whose enthusiasm for his research first convinced me to join the AT-TPC group. Thanks for his help, comments and support toward the end of this thesis. Thank you as well to the other members of my committee, Artemis Spyrou and Remco Zegers, for taking their time reading my thesis and providing helpful feedback. Again, my thanks goes to the entire AT-TPC group for the help and comments received from them. Particularly, I would like to thank Wolfang Mittig for his valuable assistance and clear explanations to understand the working principle of the AT-TPC detector. A huge thank you to Pawel Danielewicz and Paul Gueye for their mentoring, supporting, motivating, valuable comments and for challenging me to become a better scientist. Additionally thanks to the staff and faculties at NSCL. The work of this thesis would not have been possible without the learning opportunities provided by NSCL/FRIB and Department of physics and Astronomy. Special thanks to Kirsten Tollefson and her team for their good leadership. Thanks to my fellow graduate students who have helped me along the way and become my friends. Special thanks to Zachary Matheson, Terrie Poxon-Pearson and Pierre Nzabahimana. I could not be here without opportunity and training given by African Institute for Mathematical Sciences (AIMS), thanks. Finally, I am very thankful for the love and support received from my family throughout the years. Special thanks to my wife Marrie Agnes Umutesi and our kid Abia Curie ILISA, you are the best and ever, words are not enough thank you.

TABLE OF CONTENTS

LIST OF TABLES

LIST OF FIGURES

KEY TO ABBREVIATIONS

- AT-TPC : Active Target Time Projection Chamber
- NSCL : National Superconducting Cyclotron Laboratory
- FRIB : Facility for Rare Isotope Beams
- RANSAC : Random Sample Consensus Model
- HDF5 : Hierarchical Data Format
- FGUI : Friendly Graphical User Interface
- SCA : Switched Capacitor Array
- CSA : Charge Sensitive pre-Amplifier
- GET : General Electronic for TPC
- MicroTCA : Micro Telecom Computing Architecture
- CoBo : Concentration Board
- ADC : Analogue Digital Converter
- AsAds : Application-Specific Integrated Circuit and Analog to Digital Conversion
- ASIC : Application-Specific Integrated Circuit
- AGET : Architecture General Eletronics for TPC
- FPN : Fixed-Pattern Noise
- MuTanT : Multiplicity Trigger and Time
- MCH : MicroTCA Carier Hub
- μ : means
- σ : standard deviations
- CV : deviation coefficient from the mean

Chapter 1

Introduction

1.1 Background of Nuclear Physics

Considerable work in sub-atomic physics has been done, where quantum theory has been applied both in atomic physics (to interactions between nuclei and electrons) and low energy nuclear physics. In nuclear physics, the study of protons and neutrons that form the nucleus at the center of an atom and the interactions that hold them together has always been a central theme for many researchers. More effort has been done using different modern techniques at low and high energy for the analysis and mapping the nuclear landscape, to understand the forces holding nucleons into nuclei, to understand the origin of nuclear matter, and to address societal needs related to nuclear science [5]. Nuclides beyond the neutron and proton drip lines are unbound and decay by the emission of one or more neutrons or protons. The nuclear drip line corresponds to the boundary between nuclides that decay by beta-particle and neutron emission. Experimental nuclear physics play a central role in testing theories for understanding the observable physical properties, dynamics and interactions of stable and exotic nuclei. Among others these interesting properties include: cross-sections, half-life, transition probabilities, mass, decay modes, electric and magnetic moments [6].

At the National Superconducting Cyclotron Laboratory (NSCL) at Michigan State University, those studies are done with a wide variety of nuclei by using different combinations of targets with beams. Modern powerful detectors with extremely high efficiency have been developed for the study of reactions induced by secondary beams far from stability [1]. The Active Target Time Projection Chamber, or AT-TPC, is a type of detector where the gas volume is at the same time a target and a detector medium, where nuclear reactions take place. Active Target detectors have gained much attention in recent years due to their high resolution and efficieny to study reactions with very exotic nuclei [7]. With the use of low [1-10 MeV/n] to medium energies [10-100 MeV/n] [1] to extract the physical properties of nuclei far from stability, the Active Target TPC is contributing significantly to experimental nuclear science, thanks to its high luminosity without loss of resolution, low-energy detection thresholds, and enable experiment where beam intensities can be as low as 10^2 pps [7]. The analysis of the data produced by this detector required a complex computational process. The development of different tools for the analysis of data from the AT-TPC are required. This thesis describe **a software tool** written in Python language for performing the calibration of the AT-TPC electronic channels.

1.2 Literature Review

At NSCL, research on nuclear experimental physics is done using differents techniques to study nuclear reactions, such as direct reactions, nuclear fusion and resonance scattering [2]. The AT-TPC is one of the detectors with high efficiency for experiments at low energies around 0.3 MeV/n to 6.0 MeV/n [8] used at NSCL. The first results demonstrate that it is a powerful detector in this energy regime. The commissioning of this detector using standard

alpha sources and radioactive ^{6}He beams done by Suzuki et al. [2] has shown its long-term stability as well as its performance, which allowed good reconstruction of reaction kinematics. With the AT-TPC, the fusion excitation function for ^{10}Be + ^{40}Ar has been measured over the center-of-momentum energy range from 12-24 MeV. The main purpose of this experiment was to demonstrate the capability of an active-target TPC to determine fusion excitation functions for extremely weak radioactive ion beams. The obtained statistics illustrates the very high efficiency of this detector [6].

The technology of the Active Target-Time Projection Chamber has recently attracted great interest to study low-energy reactions with radioactive-ion beams, due to its high efficiency and low thresholds to detect low-energy charged-particle decays. Ahn et al. [9] showed that both of these features have been used in experiments with the Prototype AT-TPC to study α- cluster structure in unstable nuclei and 3-body charged-particle decays after implantation [9]. The analysis of data from the AT-TPC is a challenging task that requires advanced tracking algorithms with high performance and reliability. Ayyad et al. [7] developed a novel data analysis framework based on the Random Sample Consensus Model (RANSAC) algorithm. They have shown that the RANSAC algorithm provides a robust and simple particle tracking method for reconstructing the vertex and the kinematics of the reaction with good precision and efficiency.

Recently, the AT-TPC has been used to measure resonant proton scattering on ^{46}Ar by Bradt et al. [10]. The results show that the resonances observed in this experiment correspond to unbound levels in the ^{47}K intermediate state compound nucleus that one isobaric analogues of states in the ^{47}Ar nucleus [11]. Four resonances were observed: one

corresponding to the ground state in ^{47}Ar, one corresponding its first excited $1/2^-$ state, and two tentatively corresponding to $1/2^+$ resonant states in ^{47}K [10]. The development of efficient measurements techniques to achieve experimental goals with the AT-TPC are required for present and future research. In this thesis, more details on a software tool for performing the calibration of the AT-TPC electronic channels is discussed in chapter 3 and 4.

1.3 Objectives

1.3.1 General Objective

The aim of this work is to make a software tool in order to calibrate the baselines, amplitudes and times of the signals recorded by the AT-TPC pads relative to each other.

1.3.2 Specific Objectives

1 The baseline (reference) of each signal is different and needs to be compensated so that the value is 0 in the absence of a signal.

2 The amplitude of the signals vary due to variations in the gap between the mesh and the pads, the size of the pads (small or large), as well as the variations in gain of the electronics. The amplitudes of the different pads need to be calibrated so that the large pads have exactly 4 times the signal of the small pads, since the large pads are 4 times larger than the small.

3 The timing of the signals induced on the pads is exactly the same at the level of the mesh, but due to different trace and cable lengths, the signals recorded by the

electronics vary and needs to be calibrated.

1.4 Methodology

1.4.1 Computational Details

To extract physics behind the data recorded by the AT-TPC requires a multi-step analysis process. The development of a software tool written in Python language in order to calibrate AT-TPC electronic channels is the main goal of this report. Table 1.1 shows the three main characteristics of every single signal (baseline, time and maximum amplitude of the charges) as results from the developed software tool. The files used in this tool has csv extension and the details of files preparations are discussed in chapter 3.

Channel number	Baseline [ADC bins]	Times [80ns/bucket]	Amplitudes + Baselines [ADC bins]	Amplitudes-Baselines
1	343	123.378	440.613	97.613
2	484	122.613	583.312	99.312
3	360	122.6	704.229	344.229
4	354	123.372	444.203	90.203
5	345	122.665	440.741	95.741
6	325	122.525	434.316	109.316
7	368	122.04	708.109	340.109
8	325	122.563	427.956	102.956
9	334	123.257	439.886	105.886
10	440	122.707	534.446	94.446
.	.	.	.	.
.	.	.	.	.
.	.	.	.	.

Table 1.1: Sample of results from software tool with three main characteristics of signals and units of measurement.

The goal of the tool written is to calibrate the baselines , amplitudes and times of the signals, recorded on the pads relative to each other . The data used in this calibration was taken by injecting a pulse on the mesh of the AT-TPC pad plane Micromegas (see Figure 2.4). By capacitive coupling, each pad receives a pulse of the inverse polarity proportional to its surface area. The data was converted into HDF5 format, where this file contained 24

events and each event is a matrix of **10221 by 512**, for examples of spectrum from each event see Figure 1.1. The channels observed during analysis were 10221 not 10240 channels as expected and this is due to bad electronics channels. A Python class ' **pytpc.HDFDataFile**' with Python 3.62 and numpy module were used to convert HDF5 file into csv files of those 24 events. To read and manipulate these data as calibrations in this software tool, some Python modules such as numpy, scipy, matplotlib.pyplot, sys, scipy.optimize, csv and cmath were used.

Numpy is a package in Python used for Scientific Computing, used to perform different operations.The numpy array is a multidimensional array used to store values of the same datatype. Cmath was used for dealing with some calculations and complex numbers; matplotlib.pyplot was used for plotting figures and scipy.optimize was used for polynomial fitting. csv was used for reading data with csv extensions; and sys module of system-specific parameters and functions provides access to some variables used or maintained by the interpreter. Mathematical model (1.1) was used to obtain these results in order to identify the signals from the big and the small pads of the AT-TPC detector.

The three main characteristics values of the signals from all events of the pulser data were stored as csv file (see Table 1.1). The results from one event were analyzed to find the fluctuations and the distributions of the three characteristics of each signal. The same process was used for the small and the big pads. I compared the single channels chosen randomly for a measurement of all events for both small and big pads. The average calculations for all events was done for each channel and all characteristics of signals. The analysis of the results are discussed in chapter 3 and 4.

1.4.2 Signal Fitting with a Polynomial

The sensor plane of the AT-TPC consists of a mosaic of 10 240 equilateral triangles (or pads) [3] that provide the x and y information for the tracks, while the signal from each pad is sampled into a 512-sample switched capacitor array at a frequency of 12.5 MHz [10]. The AT-TPC pad system and steps for signal creation, detection, position and calculation are explained in details in chapter 2. This part, focus on methodology used to fit each signal from this detector. The signal from each pad is not symmetric as shown in Figure 1.1, therefore to calibrate the AT-TPC electronics channels, we found a function which can fit each signal in order to identify its characteristics.

$$f(x) \equiv ax^3 + bx^2 + cx + d \tag{1.1}$$

This polynomial with four parameters was chosen as the best function to fit data from electronics of the AT-TPC (see Figure 3.4), where we used data taken with a pulser, and identify those four parameters. To do so, a Python code was written to fit function to all signals from electronics channels (Figure 1.1). After fitting those signals with this type of polynomial , we extracted the position of the maximum and maximum values (Figure 3.4) for each signal for the big and small pads of this detector. Each characteristics value from each signal for the big and small AT-TPC pads are stored into a calibration file that can be used for analysis of real data and extract the physical parameters from the tracks.

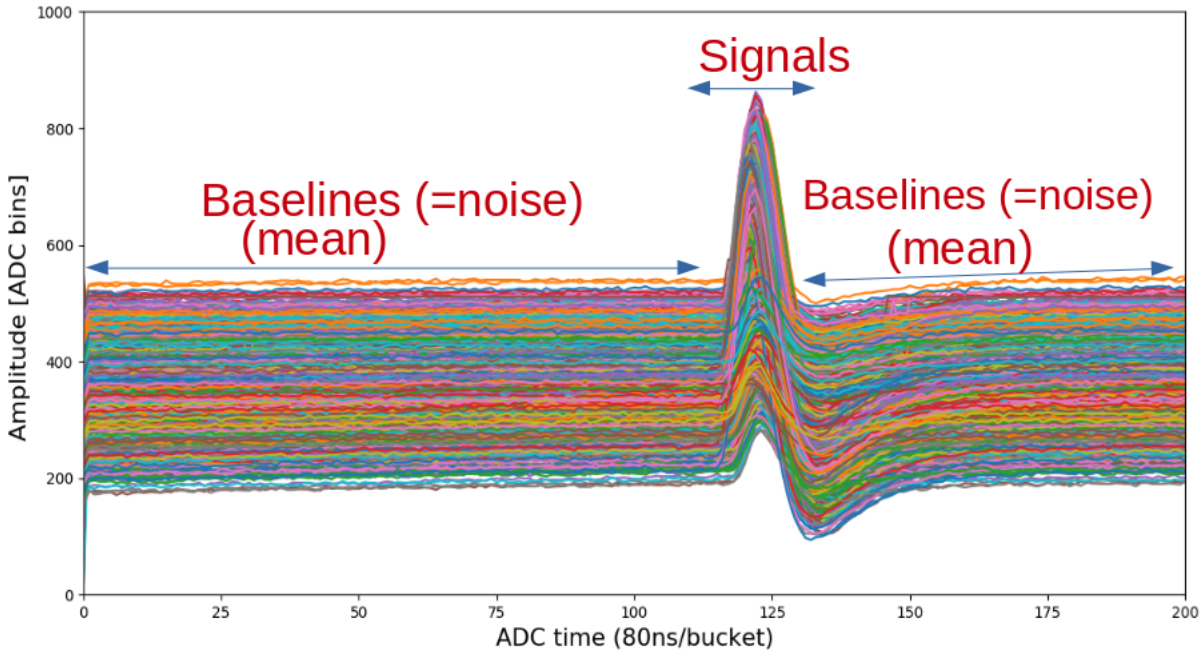

Figure 1.1: The visualization of signals from all active channels (10221) of one of the event taken from the AT-TPC pad-plane micromegas (see Figure 2.4) for data used in this work. This figure shows the various values for the height of the pulse injected on the micromesh to be calibrated in order to separate big and small pads. The signal measured on pads results from the induced current generated on pad inputs.The figure shows all signals taken during one event, where each signal is from one channel (pad) for readout of 512 time bins in x-axis. The y-axis correspond to different maxima amplitudes of charges for all signals.

Chapter 2

Active Target Time Projection Chamber Operations

At NSCL different detectors have been developed for performing experiments designed to test theories for understanding the observable physical properties, dynamics and interactions of stable and exotic nuclei. Among others these interesting properties include: cross-sections, half-life, transition probabilities, mass, decay modes, electric and magnetic moments [6].These studies are done with a wide variety of nuclei by using different combinations of targets and beams. The AT-TPC detector has been developed among others at the NSCL in order to achieve the long term technical and scientific goals of the Facility for Rare Isotope Beams (FRIB) in nuclear physics [1]. More details about the AT-TPC detector including its overview, characteristics, working principles and its electronics architecture are discussed in this chapter.

2.1 Overview of the AT-TPC

The use of time projection chambers (TPC) in low energy nuclear physics experiments has considerably increased in the last decade. Such instruments are currently used as active targets (AT), like for instance the AT-TPC, which is used both as a target and a detector for the nuclear reactions. The detection component uses the TPC operation principle, where

the inner volume of the AT-TPC is filled with a gas that is ionized by charged particles travelling through it. The same gas volume plays the role of a nuclear reaction target. It may also be used as a thick stopper for radioactive ions and as a detector for the decay products of the implanted ions, as in the case for the studies of 2-proton break-up reactions and possibly other exotic decay modes [12].

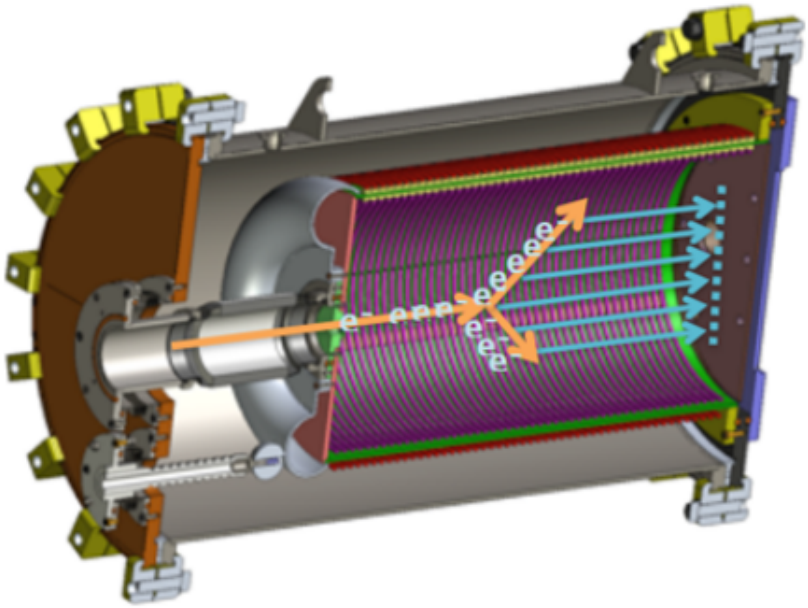

Figure 2.1: Schematic view of the AT-TPC working principle, where the inner volume is filled with gas, that is ionized by charged particles traveling through the gas toward the pad plane. The freed electrons coming from the energy loss of the particles travel through the gas toward an electron amplification device called Micromegas. The Micromegas technology was chosen in the AT-TPC as it is more tolerant to the gas and pressure variations [1]. Figure taken from [2].

The characteristics of the AT-TPC as a detector with high efficiency for experiments at low energies include: (1) a large active inner volume with dimensions defined by an electron drift region of 100 cm along the beam axis and a circular readout plane of 60 cm in diameter [3], (2) the detection of reactions at low energy with a solid angle coverage close to 4π [8], (3) a high electric field of 1 kV/cm atm for electron drift to minimize the detector

dead time in order to achieve reasonable drift velocities of the order of several cm/μs, (4) a high granularity readout plane of 10 240 channels or pads (see Figure 2.4) [7], (5) low thresholds to detect low-energy charged-particle [6], (6) waveform digitization of signals using the General Electronics for AT-TPC described in section 2.4, (7) magnetic rigidity analysis using a superconducting solenoid magnet [1], (8) the first recent application of an electron amplification technology, Micromegas , to an active target [2].

2.2 Working Principle of the AT-TPC

The incoming beam particles collide with a gas nucleus in the inner part of detector and generate reaction products (see Figure 2.1). The ionization electrons created by the charged particles traveling through the active volume drift towards the pad plane under the electric field and produce a projected image of their trucks on the surface of the Micromegas. These electrons are amplified by an avalanche process in Micromegas [2]. Each pad is connected via a decoupling capacitor of 20 nF to a charge sensitive pre-amplifier (CSA) (see Figure 2.7). A 100 MΩ resistor to ground is used to prevent the pad from floating (charging up). The signal on all pads gives directly a two dimensions projection (X, Y) of the particles tracks. The readout of the pads signal is performed by the General Electronic for TPC (GET) system (see Figure 2.6). The method used to extract the data from each signal is explained in Subsection 1.4.2, the timimg analysis is limited to the position (on time axis) of the maximum amplitude of the sampled signal of each pad. As signal from each pad is sampled in time and this information allows a digitization of the signal along the 3^{rd} dimension Z of the track [12].

2.2.1 The AT-TPC Micromegas Amplification System

Micromegas stands for MICRO-MEsh-GAseous Structure [13] and consists of a micromesh held over a segmented anode readout plane (see Figure 2.2). The gain of the AT-TPC can be varied pad by pad by applying a specific voltage to each pad. The mesh is held at a uniform distance of 128 μm above the anode plane with the help of insulated pillars placed 2 mm apart. The mesh itself is made of 18 μm thick stainless steel wire woven at a pitch of 63 μ m. The electric field applied between the micromesh and the anode plane is about 50 times higher than the one in the space between the cathode and anode. When a charged particle passes through the detector, it ionizes the gas in the drift region. The relatively low electric field in the drift region then transports the electrons toward the mesh [3]. The amplified number of electrons from the avalanches in this intense field region produce a signal that then can be read out by the electronics. Depending on the purpose of the experiment, the electron gain can be adjusted to provide amplification factors up to 10, 000 [1]. This amplification system is illustrated in Figure 2.2.

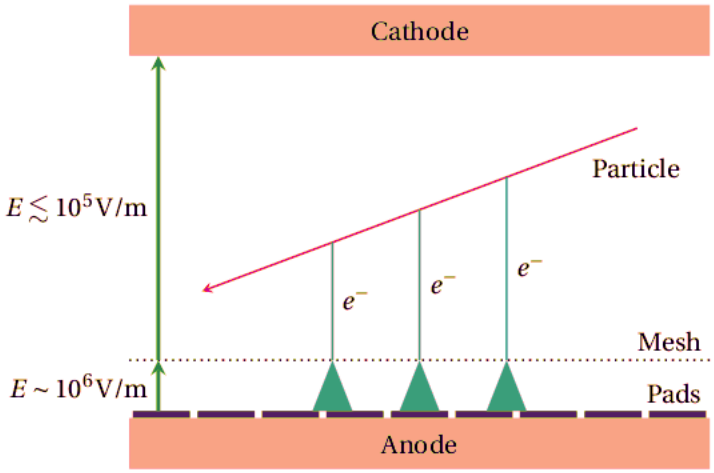

Figure 2.2: Working principle of a Micromegas. The mesh is biased with respect to the electrodes to create a large electric field between the mesh and the pads. This shows two regions: a large drift region above the mesh and a small multiplication region below the mesh. When a charged particle passes through the detector, it ionizes the gas in the drift region. The electric field magnitudes shown are nominal where the field in the region above the mesh vary from roughly 10^3 V/m to 10^5 V/m. Figure taken from [3]

2.2.2 The AT-TPC Pad Plane System

The AT-TPC detector has a sensor plane consisting of a circular printed circuit board of radius 27.5 cm covered with 10240 triangular gold-plated pads. The pads are arranged in a hexagonal inner part of 6144 small pads with height 0.5 cm surrounded by an outer part of 4096 big pads with height 1.0 cm (see Figure 2.4) [8]. In this thesis, 10221 pads were found during the analysis of data taken by injecting a pulse on the mesh of the AT-TPC pad plane Micromegas, indicating that 19 pads were missing. The missing of some pads could be due to various reasons; including bad interface contacts to the board , of bad circuit connections or damaged circuit connected to those pads.The geometry of the pad plane design was chosen to be of triangular shape in order to maximize the spatial resolution of the detector. The central region has pads 4 times smaller than the big pads.

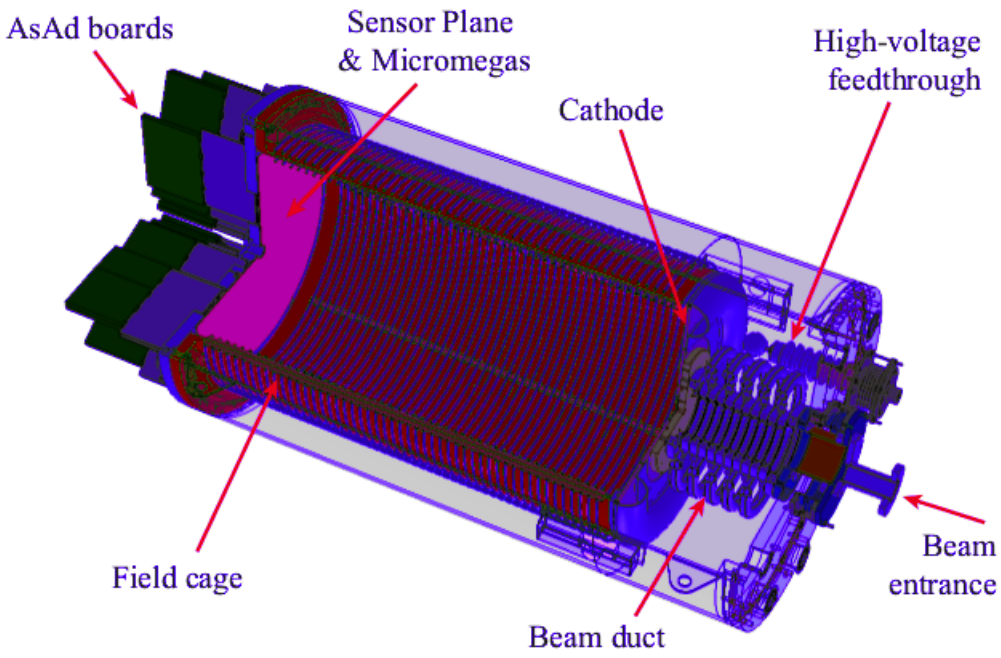

Figure 2.3: A schematic view to clarify the different components of the AT-TPC detector consists of a gas-filled vessel equipped with an anode and a cathode capable of producing a moderate electric field. The upstream end of the volume of this detector is sealed with a stainless steel cathode, which has at its center a thin foil window through which the beam enters the detector. The downstream end is closed by an aluminum flange which supports the sensor plane anode . The working principle of the GET components mounted on the downstream end of the detector is described in section 2.2.2. Figure taken from [3]

2.3 The AT-TPC Characteristics

The AT-TPC detector designed and developed at the NSCL is similar to that of the half-scale prototype AT-TPC [8]. The main differences between the two detectors are the larger size of a 250 L cylindrical gas volume, 100 cm along the beam axis of the electron drift region and the 60 cm diameter circular readout plane instead of cylindrical volume of 50 cm long, 28 cm in diameter [1], an improved sensor pad plane design in spartial and angular resolution with Micromegas of 10240 pads instead of 253 pads, and the addition of a magnetic field. The high voltage is applied across the axial direction of the TPC [7], causing the ionized electrons

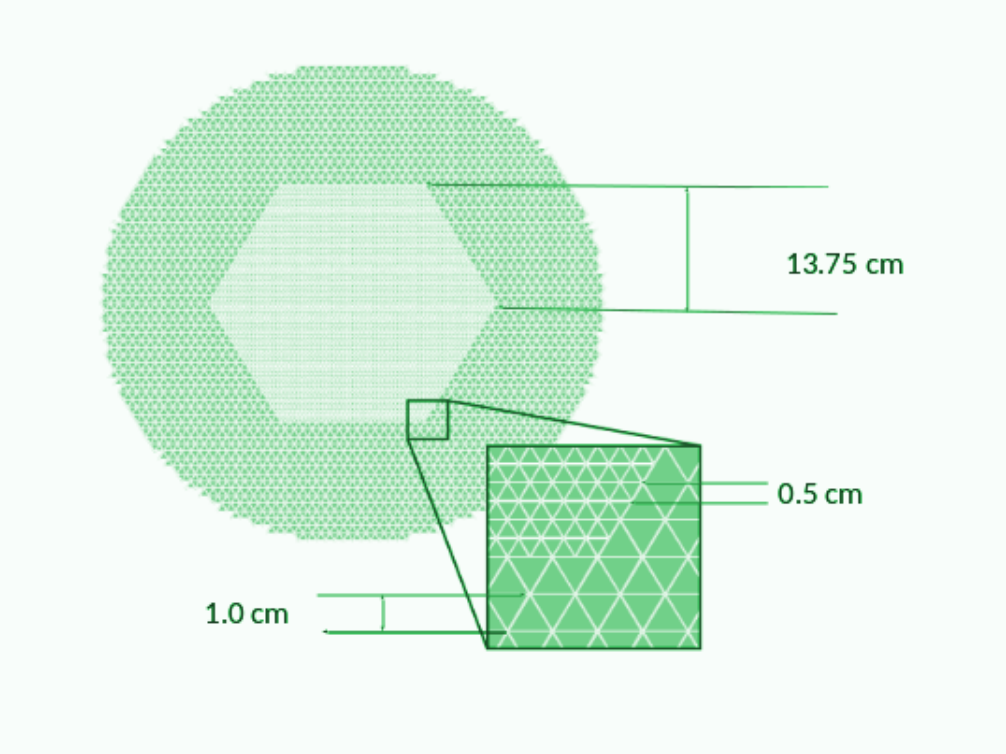

Figure 2.4: Layout of the pad plane of the AT-TPC with small pads in middle and big pads around the middle ones in order to achieve better resolution in the center region. The size of the big pads is 4 times size of the small pads. The insert shows a closer view of one corner of the hexagonal inner region chosen to preserve symmetry of image. The tool written in Python as main purpose of this thesis helps to separate those two groups of pads. Figure take from [3].

to drift toward the sensor pad plane segmented into a mosaic of equilateral triangles. The geometry of triangular pads was chosen to achieve a better resolution within small scattering angles while measuring the vertex of the reaction [1].

The high granularity of the readout pad plane of this detector allows to perform a precise magnetic rigidity analysis by using a superconducting solenoid magnet producing a field of up to 2 T. The location of these pads provide the x and y information for tracking particles, while the signal from each pad is sampled into a 512-sample switched capacitor array (SCA) at a chosen frequency between 3.125 MHz and 100 MHz [10]. The AT-TPC can optionally be tilted up to around 7^o degrees with respect the direction of the beam and the magnetic

Figure 2.5: A photography of the inner volume of the AT-TPC wall with the inner rings of the field cage installed. The outer rings of the field cage have a larger diameter and one installed on the outer surface of AT-TPC cylinder. The electric field is uniform throughout the volume of the field cage thanks to the concentric ring-shaped electrodes connected by a resistor chain that gradually steps down the voltage between each ring.

field (see Figure 2.3), in order to spread the energy of the beam over a larger area into multiple pads and avoid the saturation of the electronics on those pads [7]. Beam enters the detector through the beam duct at the right-hand side of the detector (see Figure 2.3) and then the volume filled with gas through a window ionized. The charged particles in the gas and release electrons which one then driven by an electric field toward the sensor pad plane of the detector. Nuclear reactions inside the AT-TPC can be also generated by installing a sample of target material within the detector. Traditionally, this sample is a thin foil of target material or a small amount of target material evaporated onto a thin substrate. The target can also be the TPC gas itself, creating a so-called active target [14].

2.4 Electronics Architecture of the AT-TPC

2.4.1 Overview of the GET System

The AT-TPC readout system needs an efficient waveform digitization of the signals achieved by using the General Electronics for TPC (GET) (see Figure 2.6). It features an internal discriminator for each channel, together with an internal sliding time multiplicity window, to generate a trigger for events in which the reaction products do not leave the detector [1]. In addition the GET system requires a high-density front-end with a corresponding large number of electronic channels. This system was designed to be generic for possible use in other applications. Currently, the GET system is being successfully employed in a growing number of projects using silicon and scintillating detectors such as caesium iodide (CsI), lanthanum bromide ($LaBr_3$) and cerium bromide ($CeBr_3$) for charged-particle and γ-ray spectroscopy [4].

2.4.2 Working Principle of the AGET System

The analysis of the AT-TPC data from the GET system needs to be divided in sequential steps, with the aim of extracting the relevant information from each event and transform it into the kinematic variables of interest. The electronic architecture of the GET system is divided into a hierarchy of modules to transfer the data from the detector to storage. At the lowest level of the hierarchy is a custom Application-Specific Integrated Circuit (ASIC) called the Architecture General Eletronics for TPC (AGET) (see Figure 2.6). The signals generated are sampled and shaped, then compared them to a threshold to generate a channel level trigger pulse. Through a variable-gain charge-sensitive pre-amplifier, the incoming signal is amplified, AGET stores samples of the analog signal in a switched capacitor array

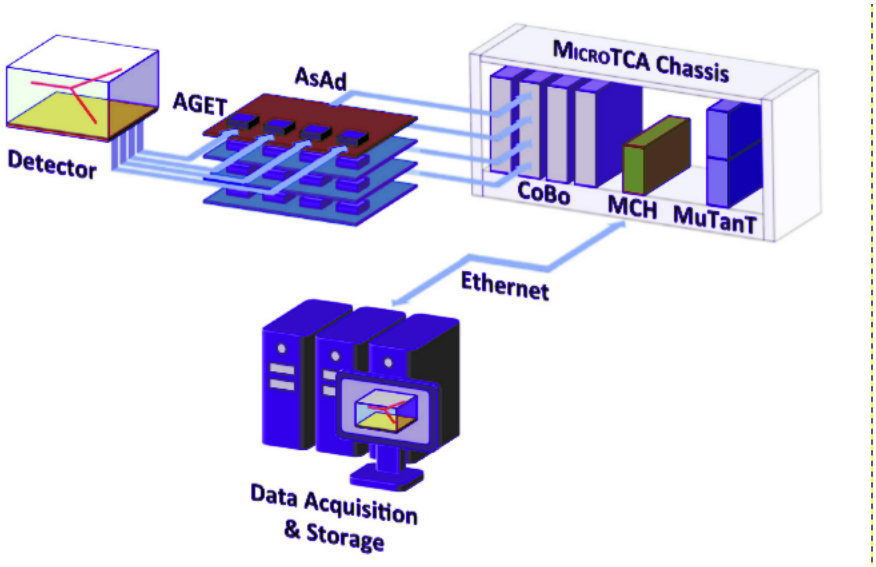

Figure 2.6: A schematic view of the GET electronic system with a single Micro Telecom Computing Architecture (MicroTCA) chassis. The MicroTCA compatible module developed for the GET system is called concentration board (CoBo). Up to 4 Analog to Digital Conversion called (AsAds) can be connected to a single CoBo and therefore one CoBo module can process data from as many as 1024 signal channels (pads). AT-TPC GET system has in total 40 AsAds therefore 10 CoBos for 10240 total channels (see Figure 2.4). Figure taken from [4]

.

(SCA) acting as an analog memory periodically where each time bucket is stored in one capacitor [4].

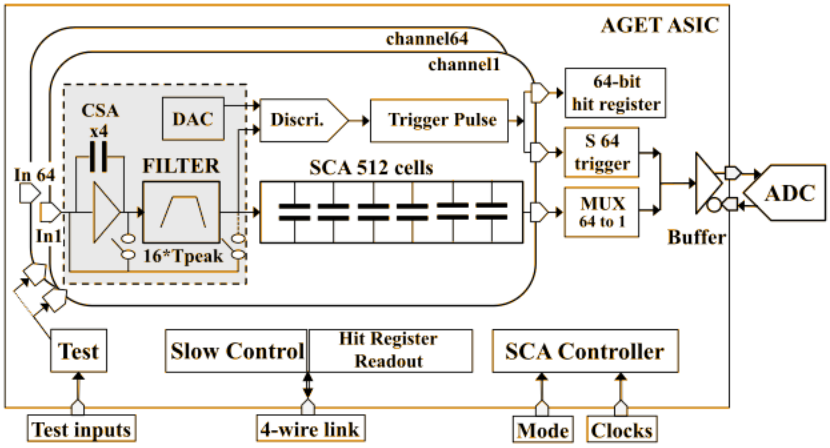

Figure 2.7: Schematic overview of Architecture of the AGET ASIC. The AGETs are mounted in groups of four on AsAd boards. Each channel integrates a charge-sensitive pre-amplifier (CSA), an analog filter (shaper), an inverting 2x gain stage, a discriminator for multiplicity building and a 512 memory-cells Switch Capacitor Array (SCA). The pre-amplifier has four different gain settings to cover dynamic ranges from maximum to minimum (120 fC, 240 fC, 1 pC or 10 pC) that can be adjusted on a channel-by-channel basis. Figure taken from [4].

The AGET chip is the front-end of the GET system that reads out the signals from 64 input physics channels to one analog output connected to an external Analogue Digital Converter (ADC), the main role of ADC is to convert analogue value to digital number. The four (4) group of AGET are mounted together on an AsAd (ASIC support and ADC) board (see Figure 2.6). The development of its architecture is described in [4] with a significant improvements to match the gain and drift time requirements, to decrease the dead time (selective readout, 1 to 512 analog memory cells see Figure 2.7) and to deal with the specific physics needs of the detector.

In order to evaluate the noise level, 4 additional channels are read the AGET chip. Those 4 channels (channels 11, 22, 45 and 56) are referred to as fixed-pattern noise (FPN) channels, they are used to measure the ambient noise. The FPN channels are distributed across the AGET to place one FPN channel on each edge of the chip. The total 16 FPN channels from 4 AGET are not connected to the detector but they are read by the Switching Capacitor

Array (SCA) in exactly the same way as the 64 input signal channels, thus allowing the data to be corrected for low frequency electronic noise. To improve the the overall resolution of the detector system, data from the FPN channels are useful offline to determine the intrinsic noise level and baseline shapes (see Figure 1.1) [15].

The main tasks of the AsAd board are to process the detector signals through the AGET, digitize the samples stored into the AGET SCA analog memory, and send these digital data to the Concentration Boards (CoBo). Up to 4 AsAds can be connected to a single CoBo and therefore one CoBo module can process data from as many as 1024 signal channels. The main task for CoBos in the MicroTCA chassis is to reduce the amount of data and to synchronize the times for all channels.

There are two communication paths for CoBo, the control path and the data path. The data path processes the raw digital data coming from the AsAd boards and sends the resulting hit-channel registers and multiplicity values to the trigger module called Multiplicity Trigger and Time (MuTanT) to generate a master trigger decision. Through the MicroTCA carrier Hub (MCH) the data is also sent via the MicroTCA backplane through an Ethernet link to external computers for data analysis and storage (see Figure 2.6) [4].

The signal stored in the memory cells of the SCA (for the channels to be read) are multiplexed and converted in parallel using a 4-channel 12-bit ADC. The extraction of signal is performed at 25 MHz frequency (the clock from the concentration boards). The obtained maximum processing time for the readout of the full SCA of 512 memory cells of the total AGET 68 channels included FPN is 1.44 ms. The physical data are transmitted to the CoBos with a maximum data rate of approximately 1.2 Gb/s (or 300 Mb/s per AGET). The processing time can be decreased by distributing the hit channels across several AGET chips. Having too many hit channels on a single AGET leads to unwanted long dead times

as described in [4]. The data extraction and conversion occur after the trigger has been accepted and once the writing in the SCA memory is complete.

The operation principles of the AT-TPC detector and its electronics architecture has been described in this chapter. A Python tool developed for calibrating the data carried by those signals is discussed in chapter 3.

Chapter 3

Graphical User Interface Tool for Calibrating the AT-TPC Electronics Channels

The analysis of the data from the AT-TPC is a challenging task that requires advanced tracking algorithms with high performance and reliability. Efficient measurement techniques are required with the AT-TPC for present and future research. A Python based software tool was developed to calibrate the baselines, amplitudes and times of each signal recorded by the AT-TPC pads. This calibration is a necessary step in the analysis of nuclear data from this detector. The working principles of this computer based tool developed for the AT-TPC detector is described in this chapter.

3.1 Files Preparations to be Used

Due to the very large number of channels and high data rate, the AT-TPC requires a custom software for data acquisition. The core of this software is written in Python 3 [3]. In order to extract the physics from the AT-TPC the data handling requires multiprocessing. They are first saved into a compact format (HDF5 file) and then converted into a csv format to be used

into the calibration tool. This is done by using the Python class ' **pytpc.HDFDataFile**' of Python 3.62 and the **numpy module**. The documentation manual provides steps for installation and use of the **pytpc package** that can be found at NSCL at **https://attpc-analysis.readthedocs.io/en/latest/**. The modules discussed in subsection 1.4.1 were used to read and manipulate these data as calibrations through multi-steps discussed in subsection 3.3 for the calibration tool. The developed Python tool is an interactive Friendly Graphical User Interface (FGUI) tool, where different files (see Figure 3.1) are needed.

3.2 AT-TPC Electronics Calibrations

Several files are needed to calibrate the AT-TPC electronics channels (see Figure 3.1). After converting each raw data (event file) with filename.h5 to filename.csv extension, then the following files are generated to be used in the calibration Python tool.

(1) The input files are the event files of the raw data needed in the same directory of the code running the developed FGUI, a sample of the output from the raw input data is the spectra shown in subsection 1.4.2 (see Figure 1.1).

(2) The pre-processed data file contains the baselines, times and maximum amplitudes of the traces. The number of such files containing pre-processed data is equal to the number of raw input files (events). They are several events in each file.

(3) Two files are created from each processed file in step 2 to store data from the big and small pads, for the purpose of the separate analysis of the signals from the corresponding pads. The results from these two files are discussed in Table 4.1.

(4) Transposed files (of the data from the big pads in all events) that contain only the

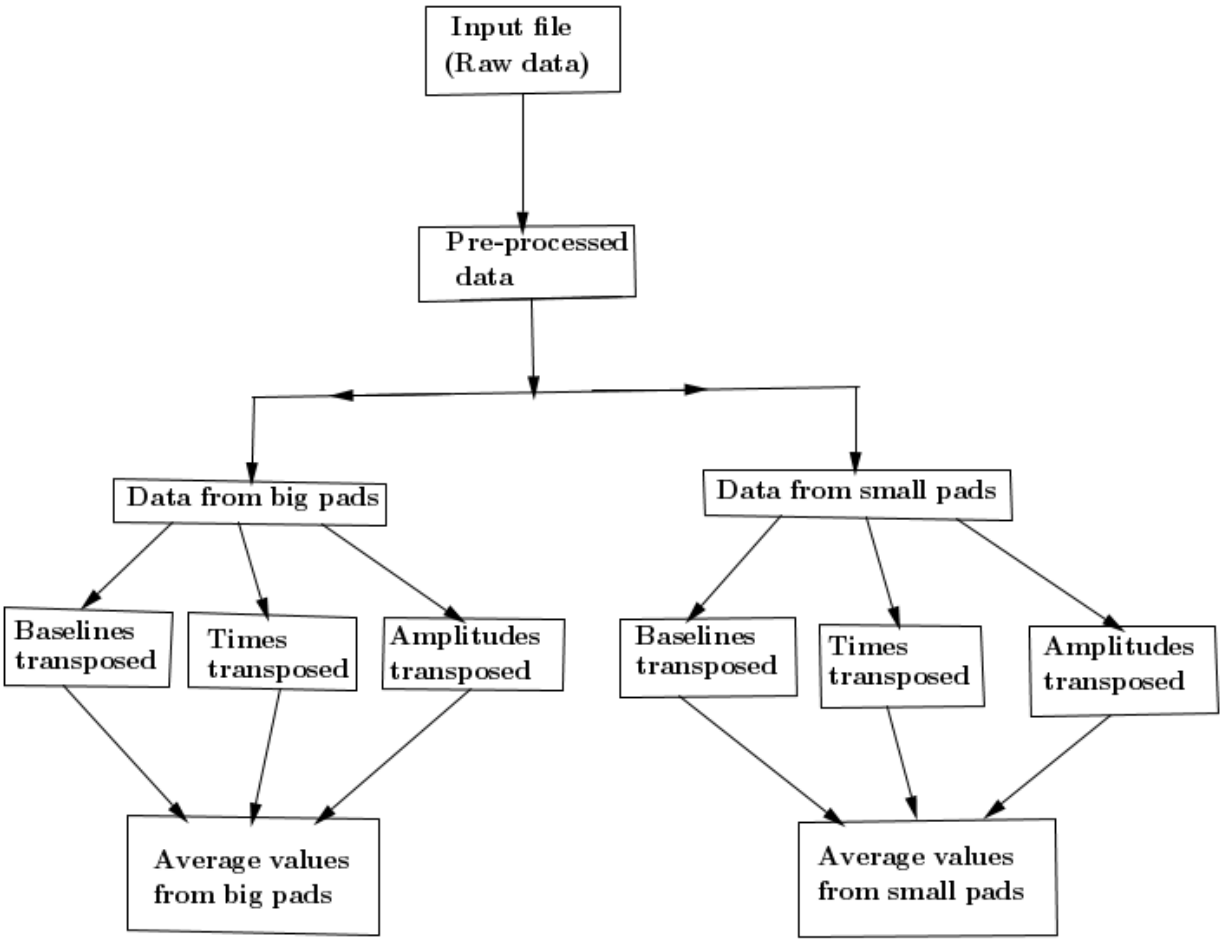

Figure 3.1: Hierarchy image of files generated to calibrate the raw data with the AT-TPC eletronic channels from the beginning (raw data) to the last file (file with average values from all events taken during the experiment).

resulting information for the baselines, the times and the amplitudes. Those files are needed for the purpose of the analysis of each characteristics of the signal, the results from these files are found in subsection 4.2.1.

(5) Same process as in (4) for the small pads.

(6) Average values of the results contains all three characteristics of each signal from the big pads for all events taken during the run. This is the last process needed for the purpose of obtaining more accurate data from the physical information of the experimental data

to be analyzed. The results from this file is found in section 4.2.

(7) Same process as in (6) for the small pads.

3.3 Functionalities of the Python Tool for the Calibration of the AT-TPC Electronics Channels

The raw data recorded by AT-TPC detector during the pulser run need to be transformed to the average data from all events taken during the run. In this work, a Python tool was created to do so.

The signals recorded from the pad plane of the AT-TPC are not symmetric as shown in Figure 1.1. Since the signals are not symmetric, we used an asymmetric function for the calibration process. In order to calibrate the electronics, each signal was fitted to analytical function described in subsection 1.4.2 in order to extract two of the three main characteristics of the signal (the amplitude and the time). The calibration process was done by using a fit function (see Equation (1.1)). This polynomial with four parameters was the best function to fit the data (see Figure 3.4) from the AT-TPC detector.

The extraction of the baselines, position of the amplitudes (times) and maximum amplitudes (see Figure 3.3 and 3.4 respectively) allows us to separate data between big and small pads. The raw data from the event file is loaded into a csv file using the Python development tool. The user of this tool can convert the compressed HDF5 into a csv using the class **pytpc.HDFDataFile**. With the use of the files discussed in section 3.1 the software tool allows the user to perform the following steps during the calibration process:

step 1: Load the input file (raw data) for each event in the form of a csv file and the output

will be the spectra of the signals recorded from one event (see the Figure 1.1). The algorithm to display every spectra from each event is given in section 4.1.

step 2: View any signal from the loaded event in order to identify the time limits for the location of the baseline and maximum amplitudes (see the Figure 3.2) used in the fitting.

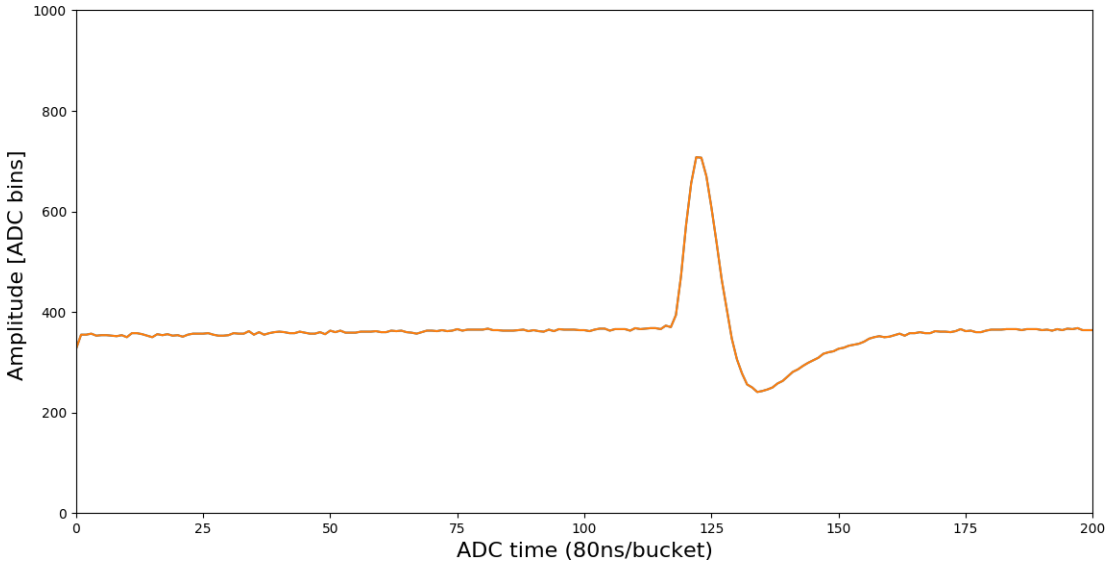

Figure 3.2: Visualization of a single signal from one of the channels (channel or pad 3) of the event 1. This sampled signal comes from the readout of the 512 cell SCA in time bins shown in x-axis, while the y-axis correspond to the amplitudes of the charges. From this signal, the information to be extracted include the baselines (noise), amplitude of each signal pulse and the corresponding time of the maximum value.

step 3: Display the value of the baseline and display it on a plot from any chosen channel by setting the time limits where the baseline is located (see the Figure 3.3). For the data used in this thesis, the time limits for the baseline are from time buckets 1 to 115.

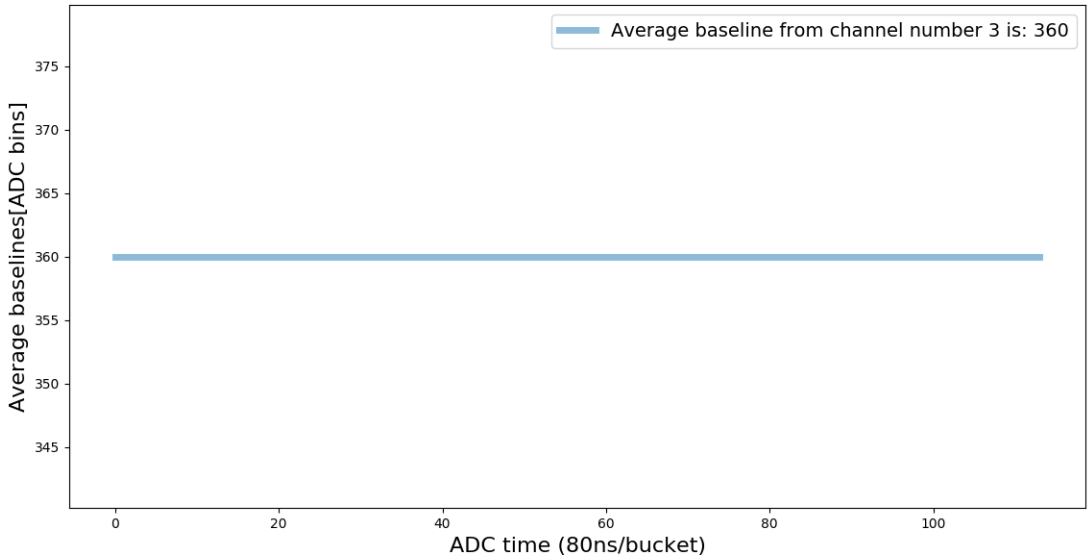

Figure 3.3: Baseline (noise) of the signal from channel (pad) 3 one of the big pads, this process was done for every single channel (10221 as shown on Figure 1.1). The time limits for the baseline are from time buckets 1 to 115.

step 4: Fitting any chosen signal to the four parameters (see equation 3.4) of the polynomial to fit the data by setting the time limits where the peak of signal is located (see the Figure 3.4). Based on the data used in this thesis, the time limits for every signal and for the fit function are from time buckets 119 to 127 and 115 to 130 respectively, this condition was applied to all signals from the small and big pads.

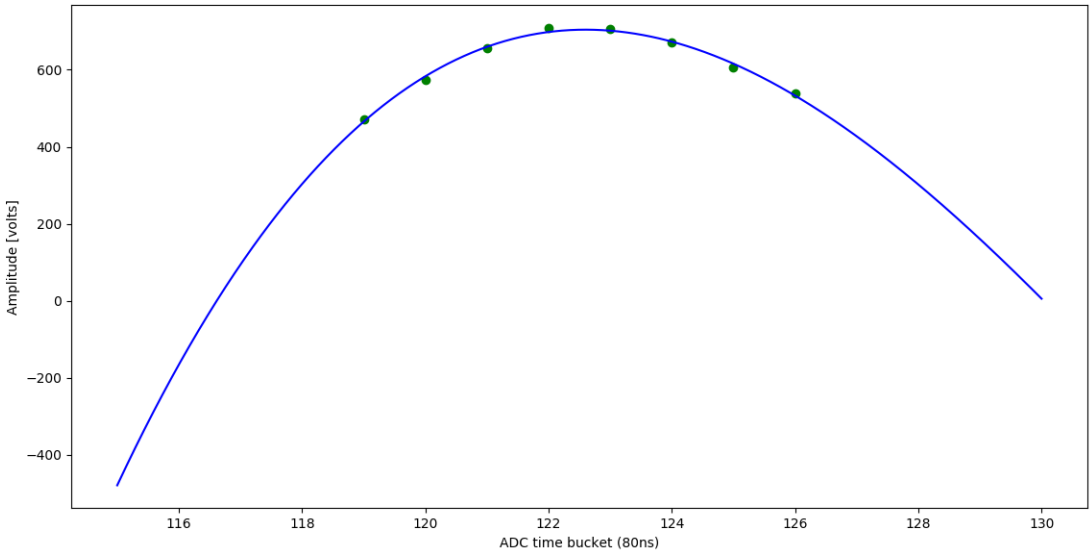

Figure 3.4: The maximum amplitude of the signal collected on the pads is proportional to the pulse injected on the mesh. To get this maximum and the corresponding time, the fit function was used to fit every signal from each event. This figure shows the signal from channel (pad) 3, where the time limits are from 119 to 127 and the time limits for the fit function is 115 to 130. This process was done for each channel (pad) of every event.

step 5: The output file.csv stores the pre-processed data (the baselines, times and maximum amplitudes of the signal) from the proceeded data of the loaded event. Then, the basic statistical parameters (means μ, standard deviations σ and deviation coefficients CV) are calculated and the fluctuations of the baseline, times and amplitudes and their distributions are evaluated. Finally, the data from the big and small pads are stored into two different output files respectively. The results from this step 5 is discussed in subsection 4.1.

step 6: The data from the file of the big pads is used to perform two main tasks for each characteristics of the signal. Firstly, it is used to determine the basic statistical parameters (mean μ, standard deviation σ and deviation coefficients CV). Secondly, is used to plot the fluctuations of the baselines, times and maximum amplitudes of the signals from

these particular data and their corresponding distributions for each event. The results from this step is discussed in Table Table 4.1**b**.

step 7: The data from the file of the small pads is treated the same way as that of the big pads as discussed in step 6. The results from this step is discussed in Table 4.1**c**.

step 8: From the result files of the baselines, times and maximum amplitudes from the data of the big pads for all events taken during the experiment, this step allows the user to calculate the basic statistical parameters from each particular channel for all measurement taken during the experiment (all events). The calculated values are stored into a new output file. The same process is applied to the data of the small pads from all events.

step 9: This step performs the analysis of the baselines, times and maximum amplitudes from any chosen channel that belongs to each of those files from the big pads of all events. To do so, the basic statistical parameters from each characteristic of signal are calculated from the corresponding files. The output file is created with those calculated statistical parameters stored for all channels. The same process is applied to the small pads. The results from this analysis is discussed in section 4.2.1

step 10: Analysis of the two files corresponding to big and small pads of the three characteristics of the signals with the average results from all events taken during the run. This step will allow the user to analyze the fluctuations of the baselines, times and amplitudes and their distributions. This analysis is discussed in section 4.2.

The 10 steps described above shows the functionalities of the developed Python tool for AT-TPC electronics channels. This tool is a friendly graphical user interface program, where

the user interacts with the computer at each step appearing on the main menu. The results from this computer based tool to calibrate the electronics channels of the AT-TPC detector is discussed in chapter 4.

Chapter 4

Data Analysis and Discussion

In order to check the performance (intrinsic resolution) of the AT-TPC electronic channels (pads plane system), the data needed in this calibration was taken by injecting a pulse on the mesh of the AT-TPC pad plane Micromegas (see Figure 2.4). By capacitive coupling, each pad receives a pulse of the inverse polarity proportional to its surface area. The calibration of the electronics channels of the AT-TPC detector requires multi-step analysis of the raw data recorded. The details of the AT-TPC pad plane system is described in chapter 2 under subsection 2.2.2. The goal of this thesis, is to develop a Python tool in order to calibrate the baselines, amplitudes and times of the AT-TPC pad signals relative to each other. The working principle and the general description of the steps toward the results from the developed Python tool is described in chapter 3. The present chapter presents the analysis of the results from the tool. The three symbols used in this chapter to assess the spread of the fluctuations and distributions of the extracted baselines, times and maximum amplitudes are: μ, σ and CV for mean, standard deviation and coefficient of variation from the mean respectively. The analysis of one event and the average results from all events is discussed in this chapter.

4.1 Results From the First Event

The energies of particles traveling in the detector can be evaluated from their energy loss along their trajectories. For that purpose, it is necessary to sum the signal amplitudes from the pads that collect the charges along each particle track. This requires to gain match the amplification of all pads. The amplification from the avalanche at the Micromegas on one side and from the read-out electronics on the other side.

Recall that the data analyzed in this thesis was taken by injecting a pulse on the mesh of the AT-TPC pad plane as shown on Figure 2.4. By capacitive coupling, each pad receives a pulse of the inverse polarity proportional to its surface area. 24 events were recorded during the run and each event is a matrix of 512 time samples by 10221 channels. The illustration of the various value for the height of the pulse injected on the mesh must be calibrated in order to separate the signals from the big and small pads (see Figure 4.1). The calibration of the AT-TPC electronics channels was done by extracting the baselines, maximum amplitudes and times. To do so, the data from one of the 24 events shown in Figure 4.1 was used.

The Python algorithm which can display the spectra of each event taken during the experiment is shown bellow.

```
Function():
   open filename as csvfile:
     read data
        define empty list to store each channel
        define empty list to store the corresponding time
        define for loop to read channel by channel:
           append each channel
           append the corresponding time
     print np.array(channels).shape
     plt.plot(time,channels)
```

Figure 4.1 illustrates the various values for the height due to pad-mesh distance inhomogeneities differences in the electronics of the pulse injected on the Micromegas to be calibrated. The signal measured on each pad results from the induced current generated by the pulse on the mesh. In order to extract the baselines, times and maximum amplitudes of every signal and calibrate the AT-TPC electronics channels, two main processes were used:

1 An average of the traces away from the pulse was performed on all channels to get the baselines. The baseline (reference) of each signal is different and needs to be compensated so that the value is 0 in the absence of a signal (see Figure 3.3).

2 A fit function described in 1.4.2, was used to extract the maximum amplitudes of the signals (see Figure 3.2) and the corresponding times.

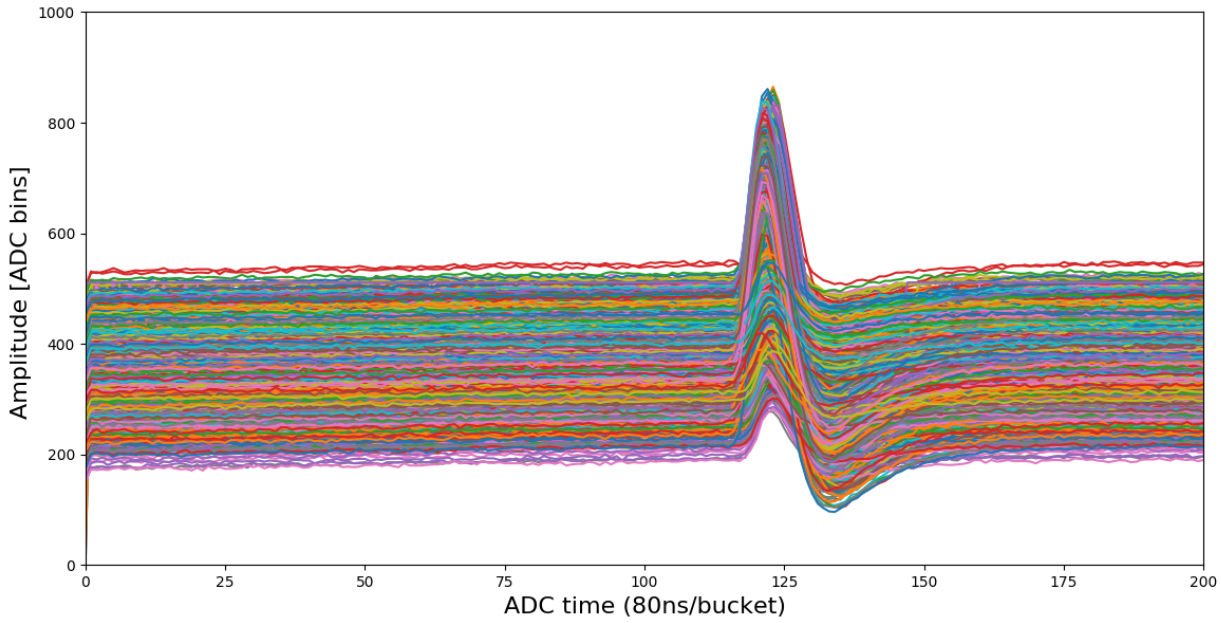

Figure 4.1: Visualization of the pad signals from one of the events collected in order to calibrate the AT-TPC electronics channels (10221 pads). See text for more details.

The signal amplitudes are different within one event, according to the position of the pads on the collection plane (gap between the mesh and the pads), the size of the pads (small or large), as well as the variations in gain of the electronics. The extracted data from the chosen event was used to find the fluctuations and distributions of the baselines, times and maximum amplitudes. The same process was repeated for the data from both the big and small pads.

4.1.1 Fluctuations of the Signal Characteristics From the First Event

After analyzing the data from the first event as described in the previous section, the values of the three characteristics of the signals (baseline, times and maximum amplitudes of charges)

were determined and stored into a comma separated value (csv) calibration file. Equation (4.1) was used to calculate the standard deviation (σ), which is a measure of the spread of the data. The coefficient of variations of the data from the mean (CV) was calculated using equation (4.2).

$$\sigma = \sqrt{\frac{1}{N-1}\sum_{i=1}^{N}(x_i - \mu)^2} \tag{4.1}$$

$$CV = \frac{\sigma}{\mu}. \tag{4.2}$$

The σ and CV in this particular analysis have the same purpose, with the only difference that σ is an absolute measure (in unit of measurement) of the observation. Because the coefficient of variation is a relative measure (measured in percent), it is easier when comparing the variation for more than one group.

The fluctuations of the data from the first event are shown in Figure 4.2 and Figure 4.3 for signals from the big and small pads. The coefficient of variation of the baselines and maximum amplitudes from their mean are 12.7%; 14% and 6%; 11.1% respectively as shown in Figure 4.2**a** and 4.2 **b**. The fluctuation of the maximum amplitudes from the big and small pads are 4% and 7.5% respectively as shown in Figure 4.2, where the baseline value was subtracted to the samples on a channel-by-channel basis in order to remove them. The fluctuations of the times is much smaller ($\sigma = 0.826 \equiv 66ns$) as indicated in Figure 4.4: this is expected as the timing of the signals induced on the pads (big and small pads) is the same at the level of the mesh, and the observed fluctuations are due to different traces and cable lengths.

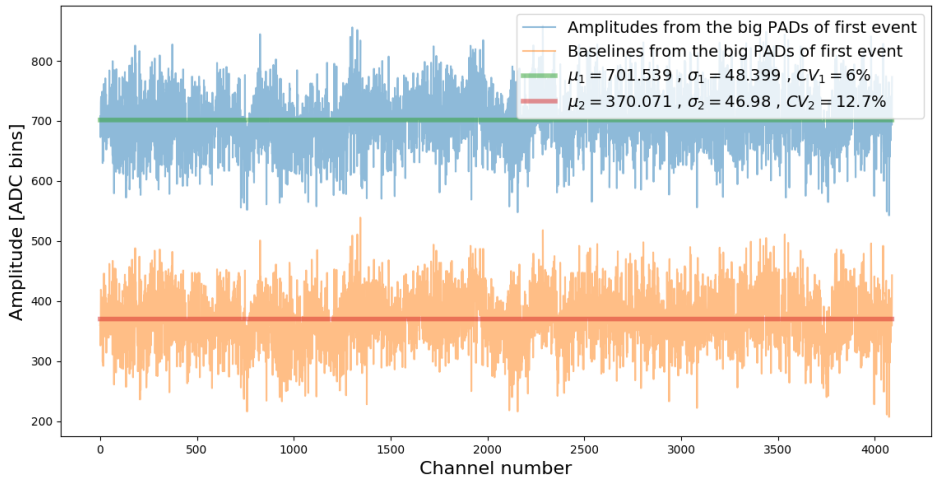

(a)

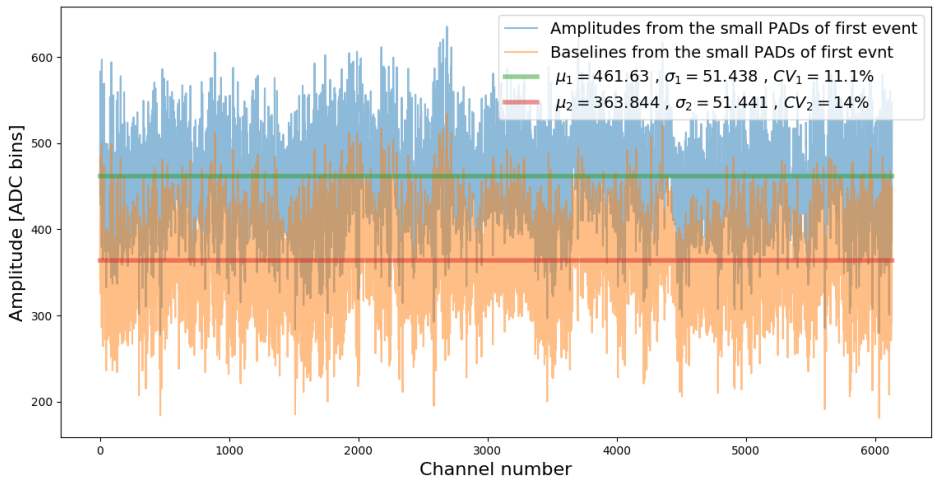

(b)

Figure 4.2: Data from the first event: (a) and (b) shows the fluctuations of the raw amplitudes in blue from the big and small pads. The green solid line shows their mean values $\mu = 701.539$ and $\mu = 461.63$ respectively. Their baselines are shown in yellow and the red solid line shows their mean values $\mu = 370.071$ and $\mu = 363.844$ respectively. The corresponding values of the σ and CV of the baselines and the maximum amplitudes from this event in this calibration process is shown in each sub-panel.

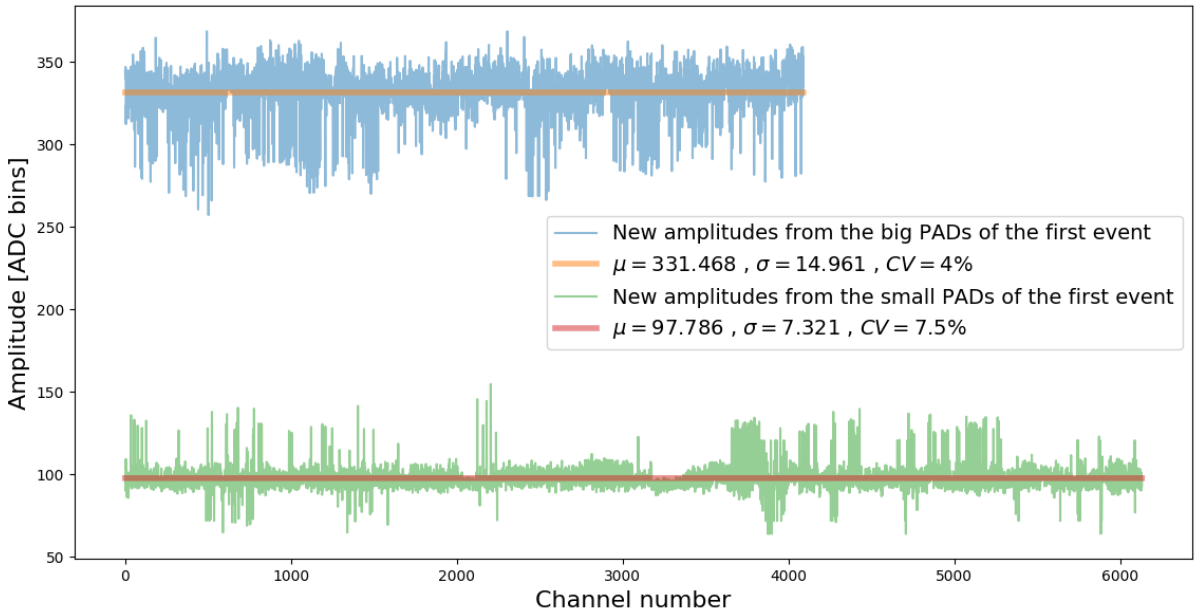

Figure 4.3: Fluctuations of the amplitudes from the big (top plot) and small (bottom plot) pads in blue and green respectively, obtained after baseline was subtracted to the samples on a channel-by-channel basis, in order to remove them. The yellow and red solid line indicate their mean values $\mu = 331.468$ and $\mu = 97.786$ respectively. The corresponding values of the σ and CV of the baselines and the maximum amplitudes from the big and small pads of this first event are shown in this Figure

4.1.2 Distributions of the Signals Parameters From the First Event

The process of extracting the data from the signals recorded by this detector was explained in details in chapter 3. After collecting the data, it was analyzed to identify signals from the big and small pads. To do so, the behavior of the distributions of the baselines, times and maximum amplitudes of the signals were analyzed by calculating the three statistical parameters (σ, μ and CV). The distributions of the baselines follow Gaussian distribution as shown on Figure 4.5 with mean μ=366.336 and standard deviation of 49.797. Those two parameters shows that the coefficient of variation of the data from the mean is 13.6%.

The times of the signals induced on the Micromegas pads are exactly the same at the level

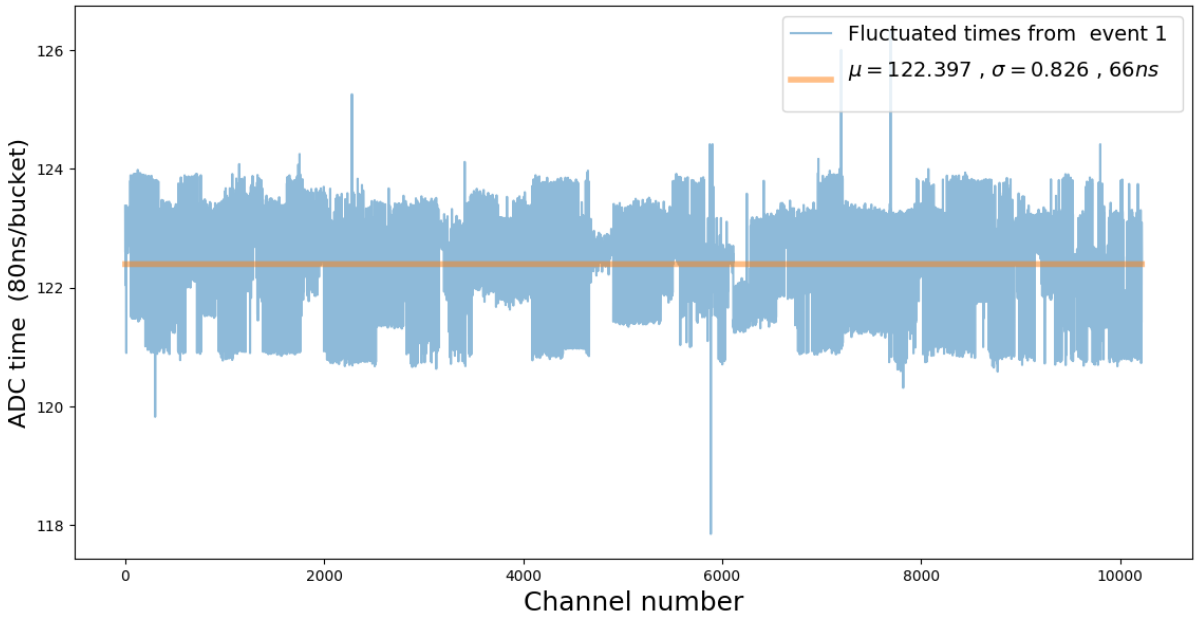

Figure 4.4: Positions (times) of the maximum amplitudes of the charges are shown with their mean (μ), standard deviation (σ) and coefficient of the variations(CV) from the mean of the data extracted from event 1.

of the mesh, but the variations are due to different trace and cable lengths. The distribution of the times has a means of 122.397 and the coefficient of variation from the means is 0.7% (with $\sigma = 0.826 \equiv 66ns$) as shown on Figure 4.6**a**. The calibrations was applied and the resulting distribution is shown on Figure 4.7**b**.

The various values of the maximum amplitudes of the signals are collected at the level of the Micromegas pads plane. The maximum amplitudes of the signals vary due to the variations in the gap between the mesh and the pads, the size of the pads (large or small), as well as the variations in gain of the electronic channels (see Figure 4.1). The methodology used to extract the various values of the maximum amplitudes of the signals corrected within one event (see Figure 4.1) is shown on Figure 3.4. In order to separate the extracted data given by the signals from the big and small pads, the distributions of the maximum values

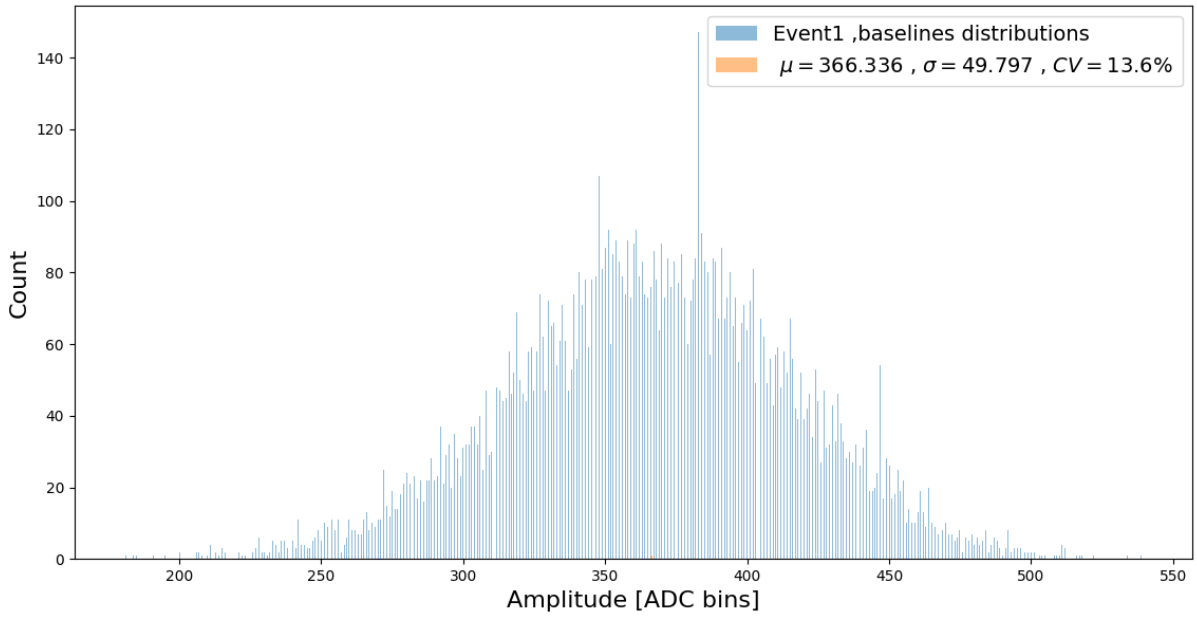

Figure 4.5: Distributions of the baselines (both big and small pads) extracted from the signals of the first event. The statistical parameters extracted from this data are: 366.336, 49.797 and 13.6% for mean, standard deviation and coefficient of variation respectively.

from the first event was used as shown on Figure 4.7**a**. The extracted data from each event are distributed normally according to the signal from the big and small pads.

The separation of those signals is done by subtracting the baselines as shown on Figure 4.7**b**. To do so, we subtracted the linear baseline to every amplitude value on a channel-by-channel basis. The statistical parameters for this particular analysis of the data extracted for the maximum amplitudes for all pads, as well as those from the big and small pads are shown in Table 4.1. Based on those statistical parameters, it is clear that the deviation of the data from the mean is smaller after calibration as indicated by the coefficients of variations.

Since the size of the large pads is 4 times larger than the size of the small pads, we expect after calibration of the maximum amplitudes extracted from the signals of the large pads

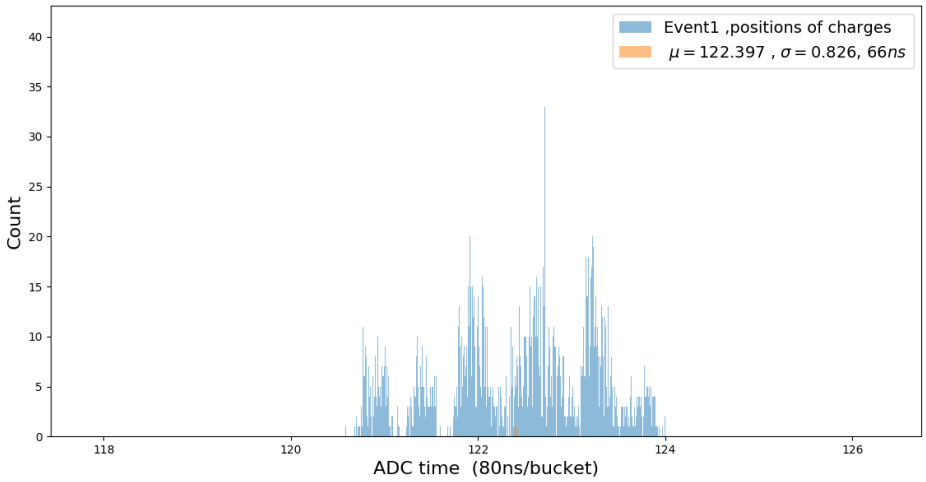

(a)

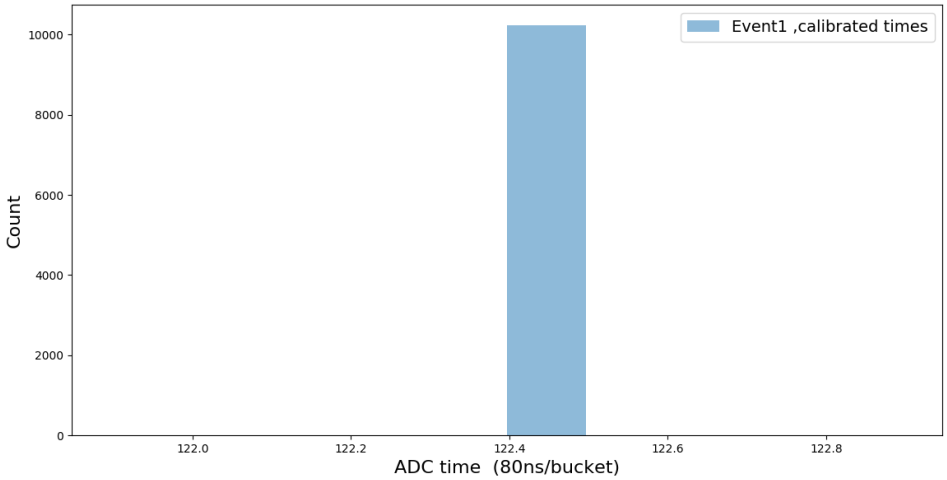

(b)

Figure 4.6: Distributions of the times of the maximum amplitudes extracted from the signals of the first event. The plot (a) shows the distribution of the uncalibrated times and the plot (b) shows the distribution of the calibtated times.

to have exactly 4 times that of the signals from the small pads (see Figure 4.8). From this analysis, we have identified the total number of the signals from the small and big pads to be 6131 and 4090 respectively. Based on this results we see that 19 pads were missing from the total number of pads 10240 (reported in [10]) of the AT-TPC pad plane. This process

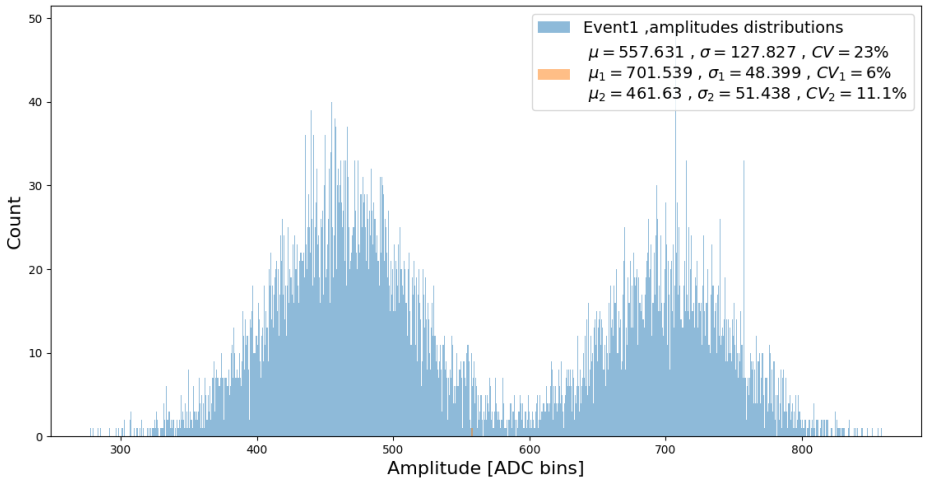

(a)

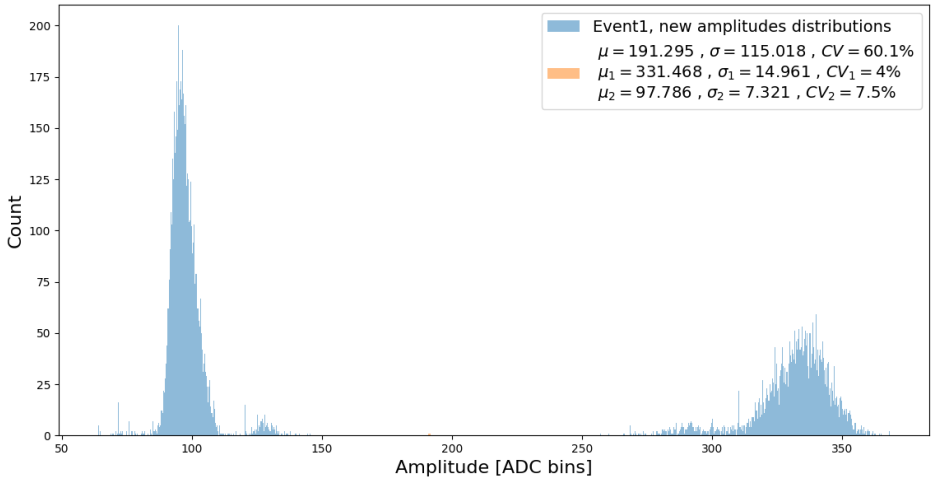

(b)

Figure 4.7: The distributions of the maximum amplitudes of the data extracted from the signals of the first event. The plot (a) shows the distributions of the uncalibrated maximum amplitudes and the plot (b) shows the distribution of the calibtated maximum amplitudes.

can therefore also be used to identify bad or missing pads prion to the experiment.

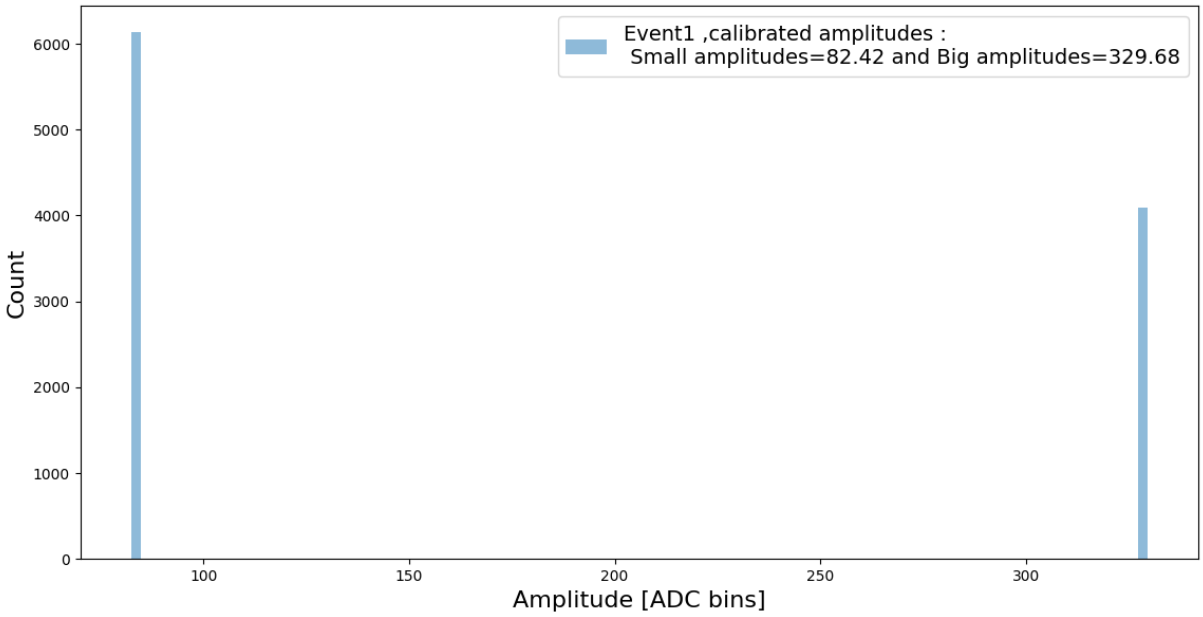

Figure 4.8: Distributions of the calibrated maximum amplitudes of the charges from the small and big pads of the first event to calibrate the AT-TPC electronics channels (10240 pads). The left side peak shows the total number of the small pads (6131) while the right side peak shows the total number of the big pads (4090) observed in this calibration.

The calibration process from the data of one event was discussed in this section, we have seen that, the fluctuations within the same group are reduced to a few %. In order to achieve a better accuracy of the informations extracted for all events, we need to discuss the results of all the three characteristics of the signals from all events taken during the run. More details about this step are discussed in section 4.2.

Characteristics of	the signals	from	the first event
	μ	σ	CV
Baselines from all pads	366.336	49.797	13%
Amplitudes + Baselines	557.631	127.827	23%
Amplitudes - Baselines	**191.295**	**115.018**	**60.1%**
Times from all pads	122.397	0.826	**66 ns**

(a)

Characteristics of	the signals	from	the big pads
	μ_1	σ_1	CV_1
Baselines from big pads	370.363	33.612	9.1%
Amplitudes + Baselines	701.539	48.399	6%
Amplitudes - Baselines	**331.468**	**14.961**	**4%**
Times from the big pads	122.229	0.871	**70 ns**

(b)

Characteristics of	the signals	from	the small pads
	μ_2	σ_2	CV_2
Baselines from big pads	364.265	32.041	8.8%
Amplitudes + Baselines	461.63	51.438	11.1%
Amplitudes - Baselines	**97.786**	**7.321**	**7.5%**
Times from the small pads	122.51	0.774	**62 ns**

(c)

Table 4.1: Statistical parameters obtained from the distribution of the signal characteristics extracted from the first event. Tables (a), (b) and (c) shows the statistical parameters of the distributions of the signal characteristics extracted from the first event, big and small pads of the same event respectively.

4.2 Average Results of the Signal Characteristics From all 24 Events

In order to have more accurate physical information extracted from the corrected signals of each event, we need to find the average of the baselines, times and maximum amplitudes. Those three characteristics are analyzed separately for the small and big pads. The analysis of the average baselines, times and maximum amplitudes of the charges from all events is discussed in this section.

4.2.1 Measurement of a Single Channel From the Big and Small Pads

Different measurements has been recorded for one channel (pad) for all events taken during the run and the mean values have been calculated for the baselines, times and maximum amplitudes. Based on the statistical parameters calculated for the baselines and the calibrated maximum amplitudes of the channels chosen randomly from both big and small pads, the fluctuations are very small. All the measurements recorded by the AT-TPC electronic channels (pads) are easily calculated using the dedicated Python tool. The indicated three statistical parameters (see Equation 4.1 and 4.2) were used in this analysis, and the analysis done for all events shows that the fluctuations within one channel are very small and smaller than the fluctuations between channels, as shown in Table 4.2.

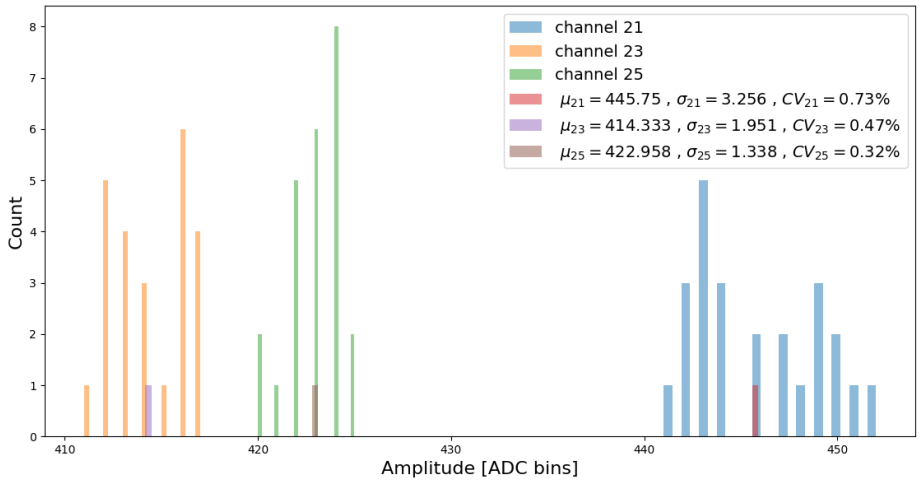

(a)

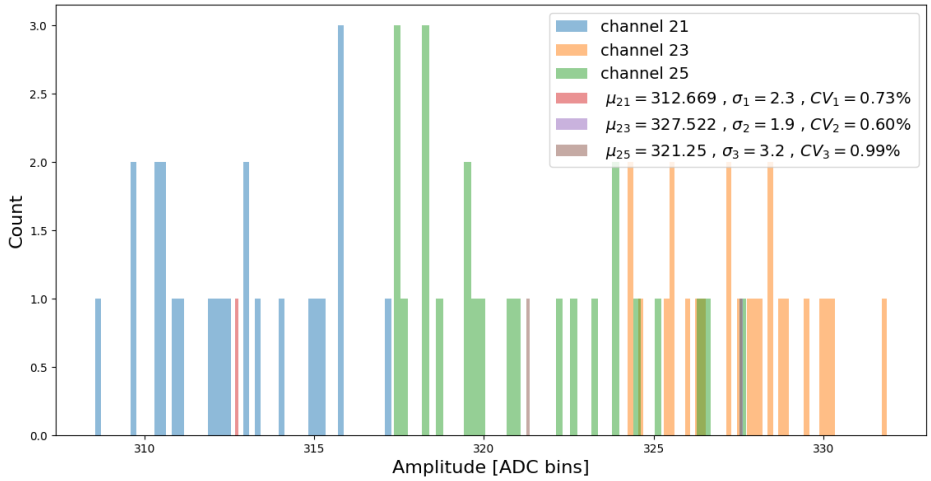

(b)

Figure 4.9: Average measurements done from randomly chosen channels from the big pads analysed for all events taken during the run. The corresponding statistical parameters are shown. The plot (a) shows the average measurement of the baselines from the three chosen channels (21,23 and 25) from the big pads. The plot (b) shows the average measurement of the corresponding maximum amplitudes.

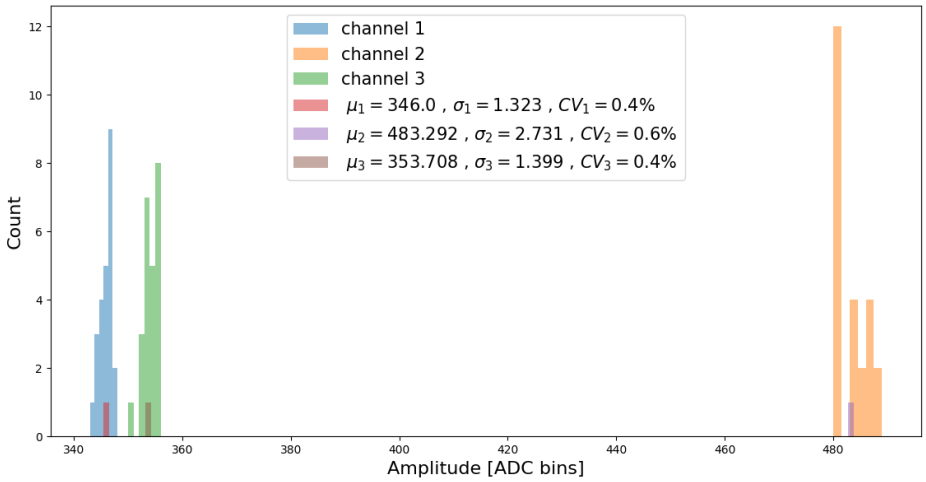

(a)

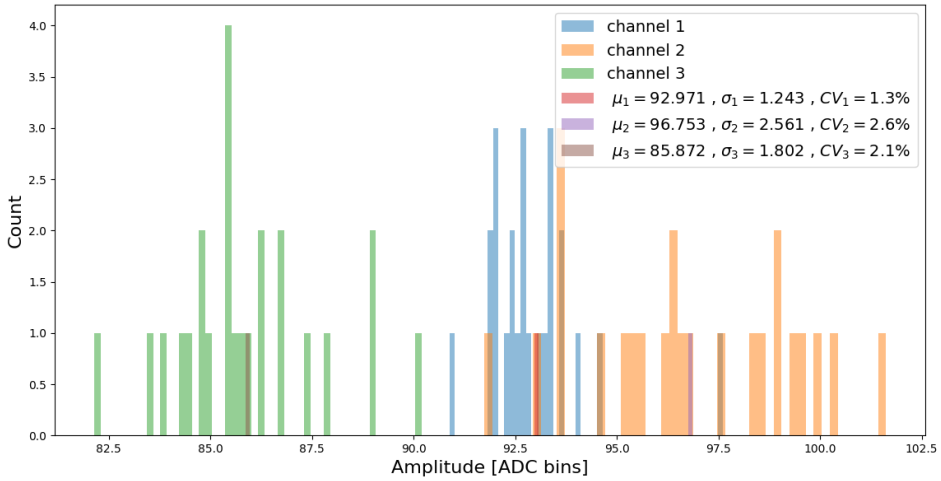

(b)

Figure 4.10: Average measurement done from a randomly chosen channels from the small pads for all 24 events analysed in this thesis. The corresponding statistical parameters are shown. The plot (a) shows the measurement of the baselines from the three chosen single channels (1,2 and 3) from the big pads. The plot (b) shows the measurement of the corresponding maximum amplitudes.

	Average measurement	from the chosen	baselines from the big pads
	μ	σ	CV
Channel 21	445.75	3.256	0.73%
Channel 23	414.333	1.951	0.47%
Channel 25	422.958	1.338	0.32%

(a)

	Average measurement	from the chosen	**amplitudes from the big pads**
Channel 21	313.669	2.3	**0.7%**
Channel 23	327.522	1.9	**0.6%**
Channel 25	321.25	3.2	**0.99%**

(b)

	Average measurement	from the chosen	baselines from the small pads
Channel 1	346	1.323	0.4%
Channel 2	483.292	2.731	0.6%
Channel 3	353.708	1.399	0.4%

(c)

	Average measurement	from the chosen	**amplitudes from the small pads**
Channel 1	92.91	1.243	**1.3%**
Channel 2	96.753	2.561	**2.6%**
Channel 3	85.872	1.802	**2.1%**

(d)

Table 4.2: Statistical parameters calculated from the average measurement of the chosen channels from the big and small pads of the AT-TPC detector. Tables (a), (b), (c) and (d) shows the statistical parameters of the distribution of the baselines, and maximum amplitudes of the three chosen channels from the big and small pads respectively.

4.2.2 Average Distributions of the Baselines From all 24 Events

The average measurements of the data extracted from all events taken during the run are needed in other to have more accurate physical information from the corrected signals. The process of correcting the average measurements is described in Section 3.1. This subsection contains a general analysis of the average measurement of the baselines corrected from all events taken during the run. The analysis of the baselines extracted from one event was shown in subsection 4.1.2. The distributions of the baselines from the average data extracted from the big and small pads of all events, follow a Gaussian distribution with mean and standard deviation of 370.363; 33.612 and 364.265; 32.041 as shown on Figure 4.11**a** and 4.11**b** respectively. All average statistical parameters calculated (σ, μ and CV) for the baselines from the big and small pads are shown on Table 4.3. The baselines coefficients of variations from the mean for the big and small pads are 9.1% and 8.8% respectively. This shows that the fluctuations of the baselines are small compared with the overall mean for both big and small pads.

	Average measurement	of the baselines	from all events
	μ	σ	CV
Baselines from all big pads	370.363	33.612	9.1%
Baselines from all small pads	364.265	32.041	8.8%

Table 4.3: Statistical parameters calculated from the average measurement of the baselines extracted from the signals of all 24 events from both big and small pads recorded by the AT-TPC detector during the pulse run.

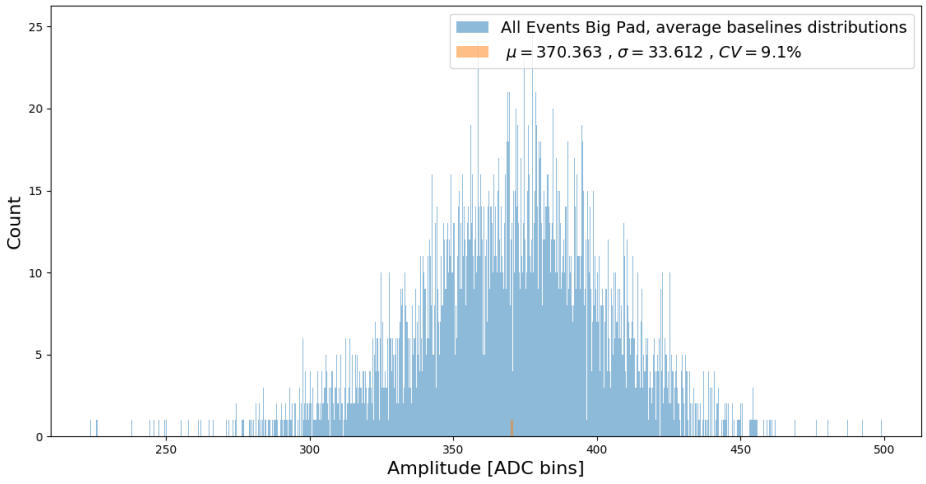

(a)

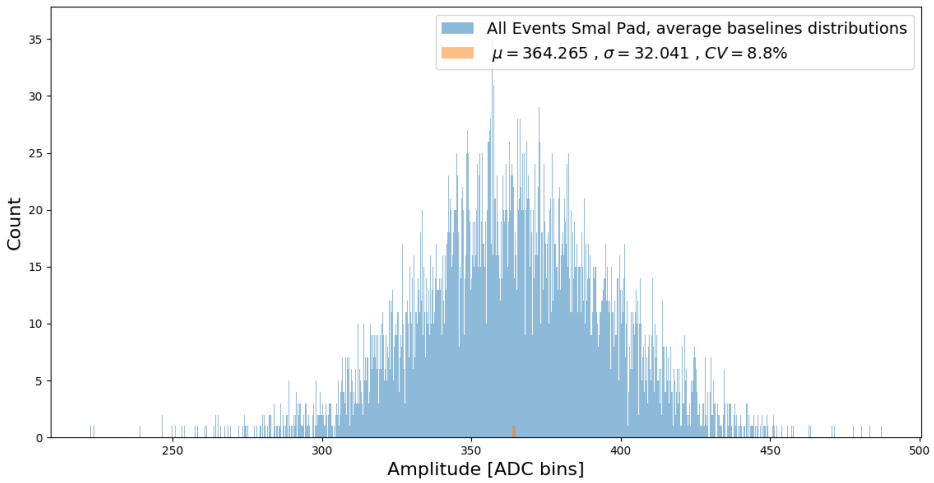

(b)

Figure 4.11: Average measurement of the baselines from the big and small pads for all events (24) analysed in this thesis. The corresponding statistical parameters are shown. The plot (a) shows the average measurement of the baselines from the big pads. The plot (b) shows the average measurement of the baselines from the small pads.

4.2.3 Average Distributions of the Positions From all 24 events

The model used to extract the maximum and its position values for each signal from all 24 events taken from the big and small pads of this detector was explained in 1.4.2. The

average measurements of the times extracted from all 24 events have been calculated, the distribution of the times have a mean of 122.397 and standard deviation of 35 ns as shown on Figure 4.12. The fluctuations of the average times is very small as expected, this is shown by the values of the standard deviations obtained from the means for both big and small pads, which are $45ns$ and $35ns$ respectively as shown on Table 4.4.

	Average measurement	of the times	from all 24 events
	μ	σ	$Times(ns)$
Times from all 24 events	122.397	0.440	$35ns$
Times from all big pads	122.237	0.558	$45ns$
Times from all small pads	122.504	0.430	$34n$

Table 4.4: Statistical parameters from the average measurement of the times extracted from the signals of all 24 events taken by the AT-TPC detector.This table shows the average statistical parameters from the distributions of the times for all 24 events, the big and small pads.

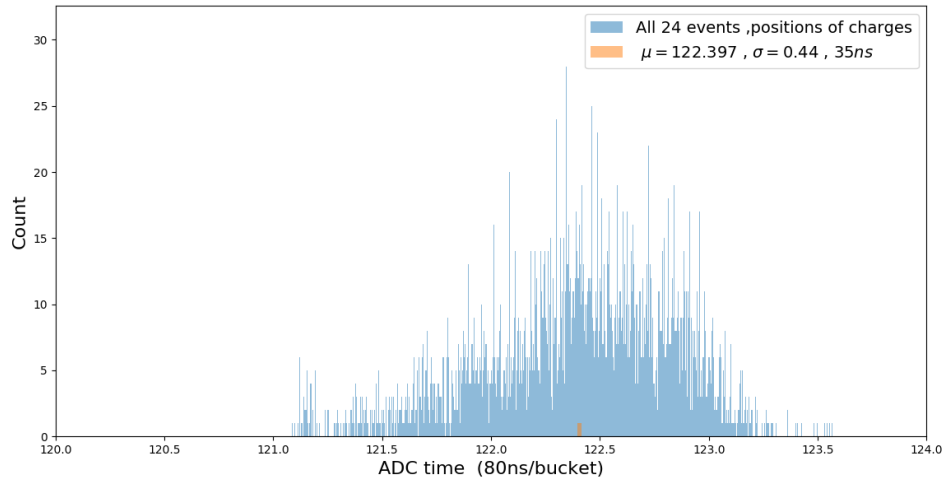

(a)

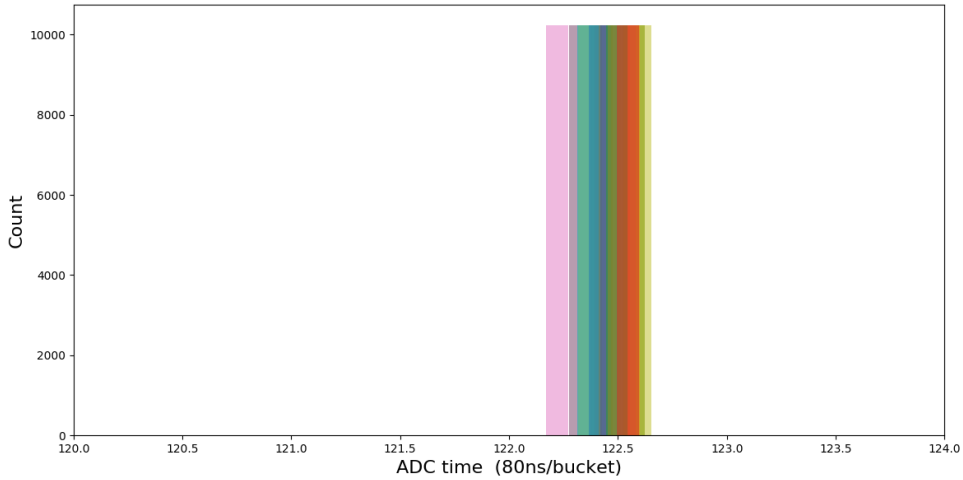

(b)

Figure 4.12: Average distributions of the positions of the maximum amplitudes from all 24 events. The plot (a) shows the distribution of the uncalibrated times and the plot (b) shows the distribution of the calibtated times.

4.2.4 Average Distributions of the Amplitudes from all 24 Events

The average maximum amplitudes of the data extracted from all 24 events taken for this particular run are analyzed in this subsection. The distributions of the maximum amplitudes of the data extracted from the big and small pads for all events follow a Gaussian distribution

with mean and standard deviation shown on Figure 4.11. The three average statistical parameters (σ, μ and CV) of the calibrated maximum amplitudes from the big and small pads are shown on Table 4.5. The coefficients of variations of the baselines from the mean of the big and small pads are 3.43% and 4.8% respectively. This shows that the fluctuations of this average data are similar and with the required resolution of 5%.

Average measurement from	amplitudes of	24 events
μ	σ	CV
Amplitudes from all big pads	327.49	11.24	3.43%
Amplitudes from all small pads	94.062	4.514	4.8%

Table 4.5: Statistical parameters from the average measurement of the calibrated maximum amplitudes extracted from the signals of all 24 events taken by the AT-TPC detector.This table shows the statistical parameters of the distributions of the amplitudes from the big and small pads for all events.

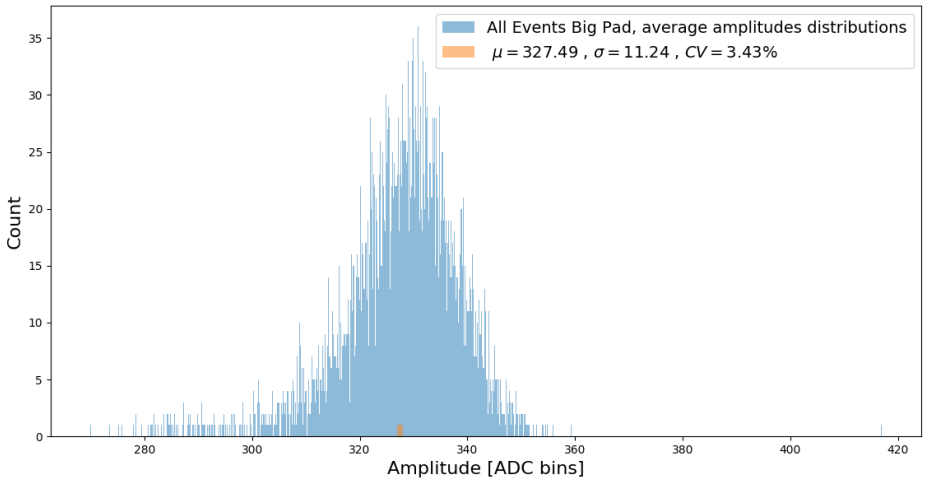

(a)

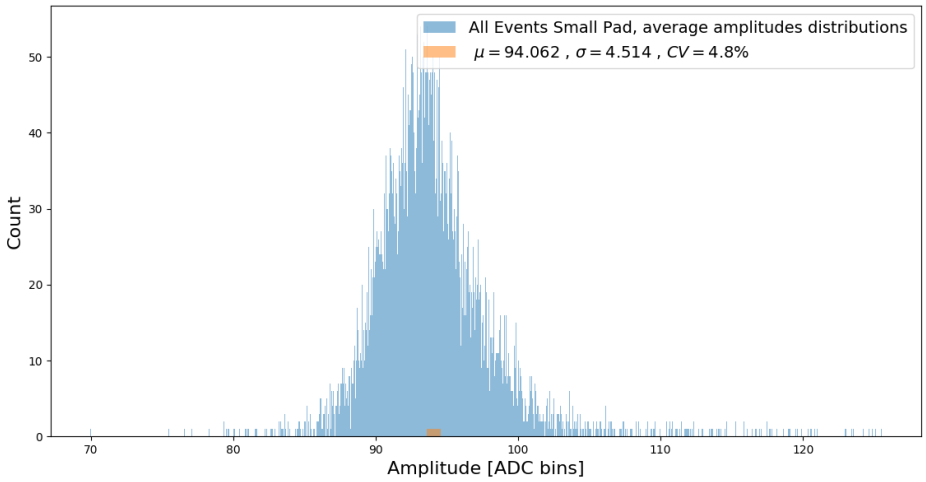

(b)

Figure 4.13: Average distributions of the calibrated maxima amplitudes from big pads in all 24 events are shown with their means (μ), standard deviations (σ) and coefficients of variations (CV) from the mean of the amplitudes.

Chapter 5

Conclusion

At NSCL, research on nuclear experimental physics is done using differents techniques of nuclear reactions, such as direct reactions, nuclear fusion and resonance scattering. The AT-TPC detector has been developed among others at the NSCL in order to achieve the long term technical and scientific goals of the Facility for Rare Isotope Beam (FRIB) in nuclear physics. The analysis of the data from the AT-TPC is a challenging task that requires advanced tracking algorithms with high performance and reliability. The development of efficient measurements techniques to achieve the experimental goals of the AT-TPC are required for present and future research. We have developed **a software tool** written in Python language for performing the calibration of the AT-TPC electronic channels. The goal of the developed tool is to calibrate the baselines, maximum amplitudes and times of the signals (see Figure 4.1) recorded on the pads relative to each other. This calibration tool is a necessary step in the analysis of nuclear data from the AT-TPC detector. The three characteristics of each signal from each pad are stored into a calibration file. The data used to develop the calibration tool of this detector, was taken by injecting a pulse on the mesh of the AT-TPC pad plane Micromegas. By capacitive coupling, each pad receives a pulse of the inverse polarity proportional to its surface area.

The file of the raw data collected by the AT-TPC detector is saved in Hierarchical Data Format (HDF5), where this file contains several events and each event is a matrix of **512** time samples by **10240** channels. A Python class **pytpc.HDFDataFile** with Python 3.62 and **numpy module** is used to convert the HDF5 file into csv files to be used in the Python tool developed to calibrate the electronics channels of this detector. To read and manipulate this data, some Python modules such as numpy, scipy, matplotlib.pyplot, sys, scipy.optimize, csv and cmath were used. A polynomial function (see Equation 1.1) was used in order to extract the times and maximum amplitudes from each signal. With the use of this model and the developed Python tool, we are able to identify the signals from the big and the small pads of the AT-TPC pad plane (see Figure 2.4). Based on the statistical analysis of the parameters calculated from every signal and the average measurement done for the data extracted within the same group of pads (the big and small pads) for all events, the fluctuations from the mean is within the required resolution of 5%. The details of the functionalities of the developed software tool written in Python language for performing the calibration of the AT-TPC electronic channels are described in chapter 3. The tool is user friendly and accessible via a graphical user interface for present and future users of this detector.

APPENDICES

APPENDIX A: Additional graphs from the First Event

A1. Fluctuations of the Maximum Amplitudes of the First Event

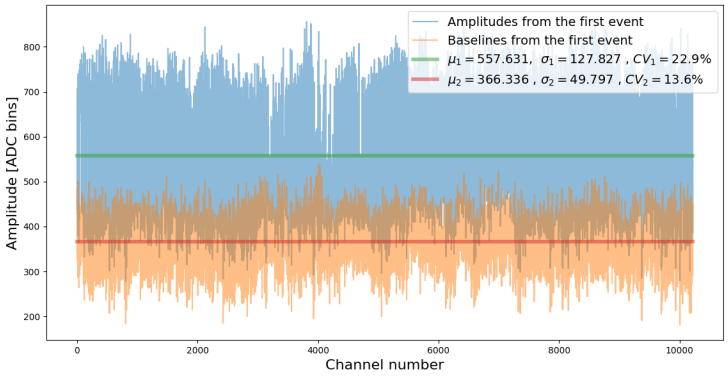

(a)

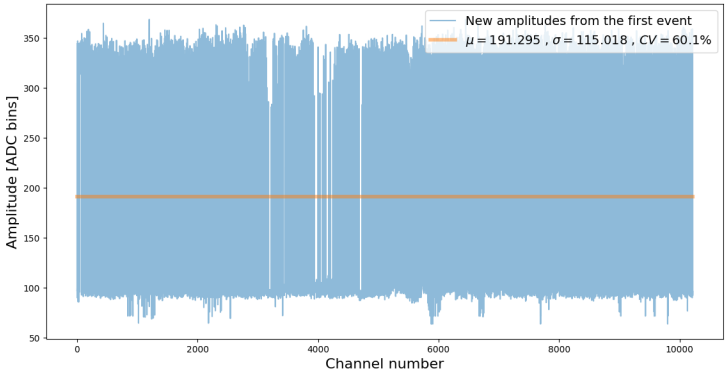

(b)

Figure A1: First event: (a) fluctuations of the raw amplitudes in blue. The green solid line shows their mean value $\mu = 557.631$. The baselines are shown in yellow and the red solid line shows their mean value $\mu = 336.336$; (b) amplitudes in blue is obtained after baseline was subtracted to the samples on a channel-by-channel basis, in order to remove them and the yellow solid line indicate their mean value of $\mu = 191.295$. The corresponding values of the σ and CV of both the baselines and maximum amplitudes are shown in each sub-panel.

A2. Distributions of the Maximum amplitudes from the Big and Small Pads

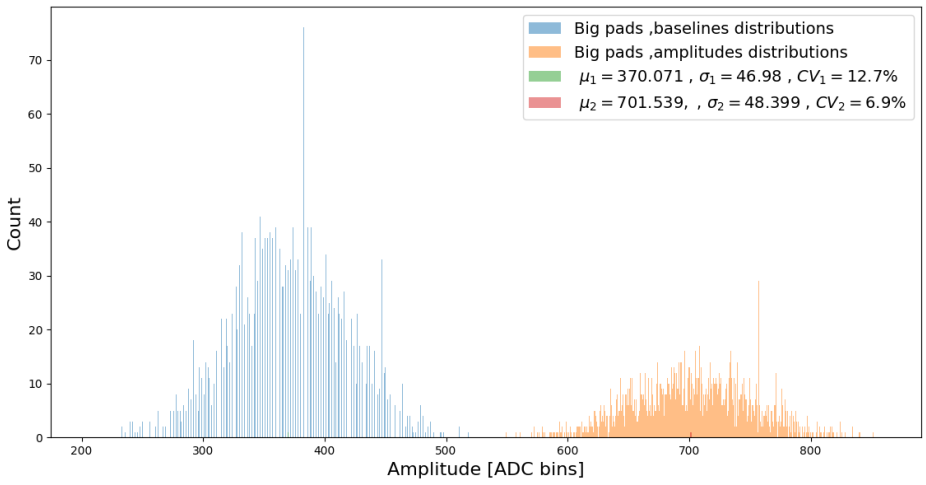

(a)

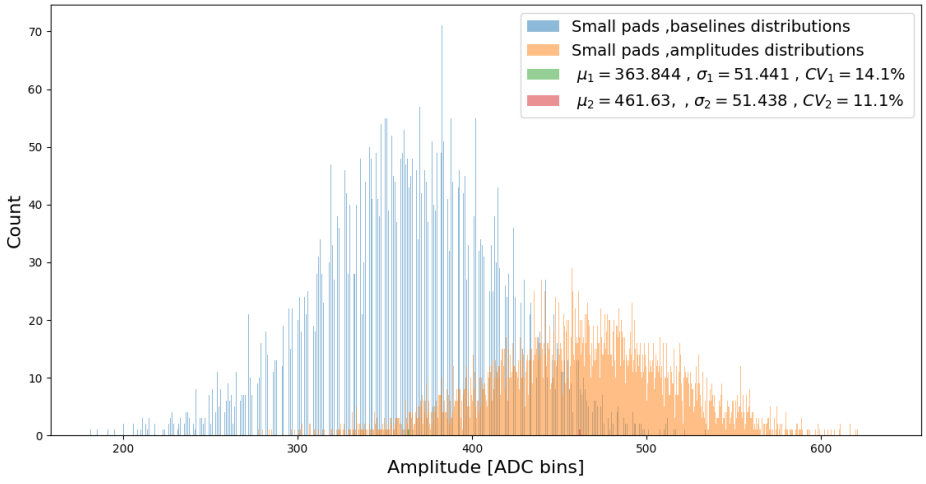

(b)

Figure A2: Distribution of the maximum amplitudes extracted from the signals of the big and small pads of the first event. Their corresponding statistical parameters are shown on each Figure. The plot (a) shows the distribution of the maximum amplitudes extracted from the data of the big pads. The plot (b) shows the distribution of the maximum amplitudes extracted from the data of the small pads.

A3. Fluctuations of the Times from the Big and Small Pads

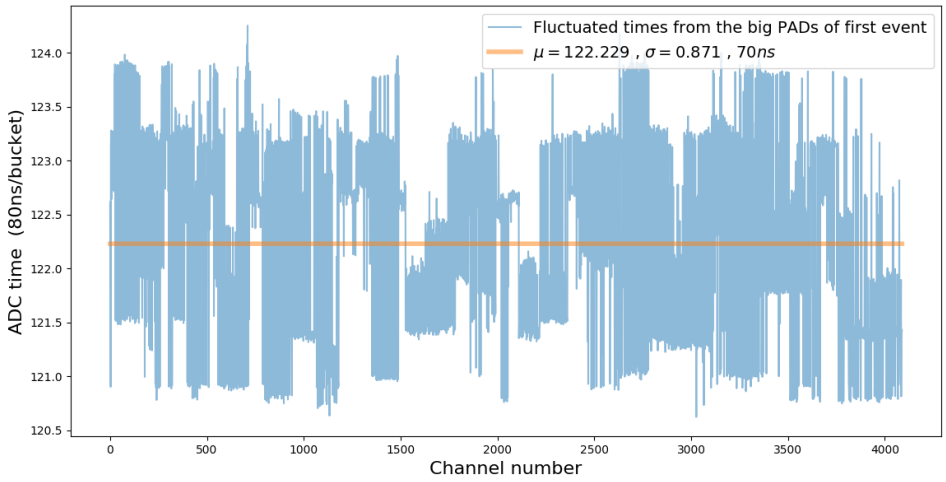

(a)

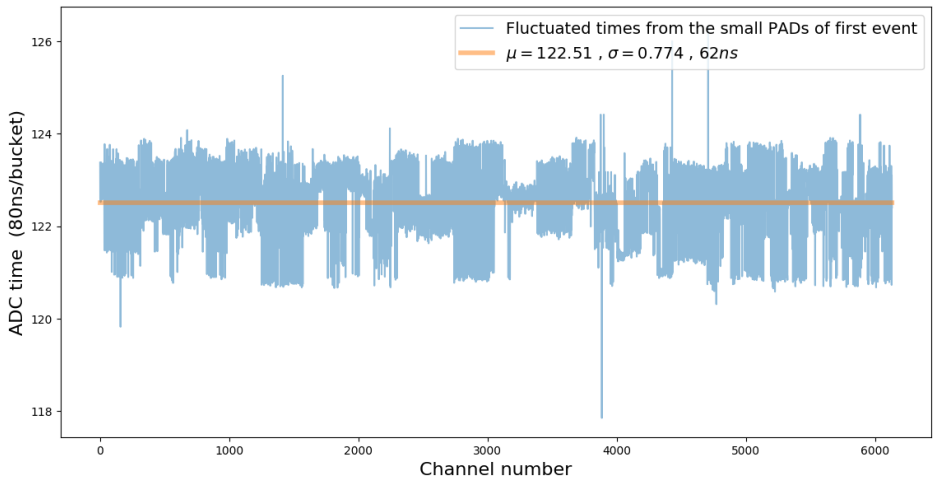

(b)

Figure A3: Fluctuations of the times from first event: (a) and (b) shows the positions (times) of the maximum amplitudes from the big and small pads in blue, their coeficients of variation from the mean are 0.7 and 0.6 respectively. Their standard deviations and means in yellow solid line are shown in each sub-panel.

A4. Distributions of the Times from the Big and Small Pads

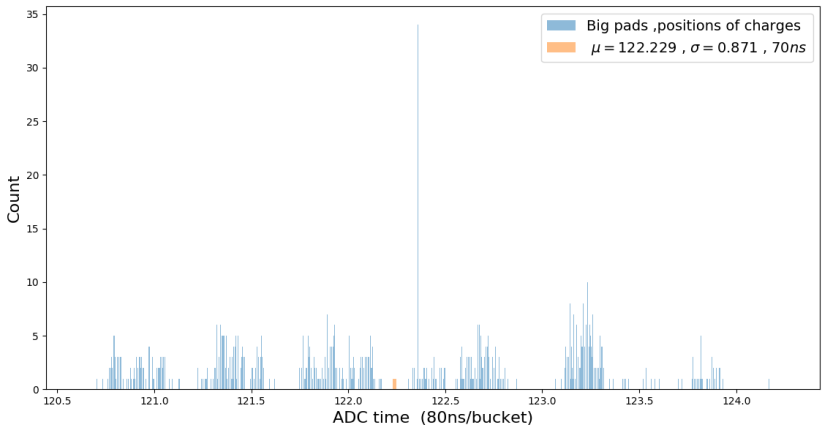

(a)

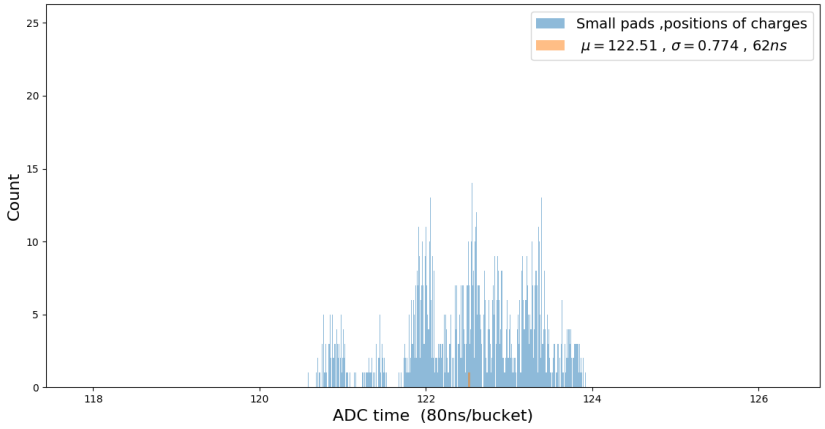

(b)

Figure A4: Distributions of the times extracted from the signals of the big and small pads of the event 1. Their corresponding statistical parameters are shown on each Figure. The plot (a) shows the fluctuations of the times extracted from the data of the big pads. The plot (b) shows the fluctuations of the times extracted from the data of the small pads.

APPENDIX B: A Friendly User Interface Tool to Calibrate the AT-TPC Electronics Channels

Different steps showing the functionalities of the developed Python tool for the AT-TPC electronics channels are shown in this part. As discussed in chapter 3, this tool is a friendly graphical user interface program, where the user interacts with the computer at each step appearing on the main menu. The results from this computer based tool to calibrate the electronics channels of the AT-TPC detector was discussed in chapter 4. Different functions defined to do a particular task have been combined and make a main menu to display on the computer screen the main steps needed by the user of this tool once open it will interact with the computer.

```
def main_menu():
menu_text = """
             Calibration of the AT-TPC Electronics Channels:
     Chose one and press enter to proceed (Done by FELIX.N under guidance Daniel.B).
[1] Load a csv file of any event
[2] View any signal from the loaded event
[3] View Baseline Value and its plot
[4] Fit any Chosen Signal
[5] Create an outfile.csv and Store Pre-Processed Data from the Loaded file
[6] Statistical Parameters from the Pre-Processed Data of the Loaded Event
[7] Fluctuations, Distributions from Extracted Data of Loaded Event and Separate them
[8] Statistical Parameters from the File of the BIG PADs
```

[9] Fluctuations and Distributions of the Signals from the BIG PADs

[10] Statistical Parameters from a File of the SMALL PADs

[11] Fluctuations and Distributions of the Signals from the SMALL PADs

[12] Matrix elements from the File of Baselines of data from the BIG PADs

[13] All statistical Parameters from the File of the Baselines of the BIG PADs

[14] Baseline Analysis from a Single Channel of the BIG PADs (All Events)

[15] Matrix Elements from a File of the Times from the BIG PADs (All Events)

[16] All Statistical Parameters from the File of the Times of the BIG PADs

[17] Time Analysis from a Single Channel of the BIG PADs (All Events)

[18] Matrix Elements of the File of the Calibrated Amplitudes from the BIG PADs

[19] Statistical Parameters from the file of calibrated amplitudes from BIG PADs

[20] Amplitudes Analysis from a Single Channel of the BIG PADs (All Events)

[21] Matrix elements of a file of the Baselines from the SMALL PADs (All Events)

[22] All statistical Parameters from the file of the Baselines from the SMALL PADs

[23] Baseline Analysis from a Single Channel of the SMALL PADs (All Events)

[24] Matrix Elements of a File of the Times from the SMALL PADs (All Events)

[25] All Statistical Parameters from the File of the Times from the SMALL PADs

[26] Time Analysis from a Single Channel of the SMALL PADs (All Events)

[27] Matrix Elements of the File of the Calibrated Amplitudes from the SMALL PADs

[28] Statistical Parameters from the File of Calibrated Amplitudes from SMALL PADs

[29] Amplitudes Analysis from a Single Channel of the SMALL PADs (All Events)

[30] Statistical Parameters from a File of the AVERAGES BIG PADs (All Event)

[31] Fluctuations and Distributions from the File of AVERAGES BIG PADs

[32] Statistical Parameters from a File of AVERAGES SMALL PADs (All Events)

[33] Fluctuations and Distributions from the File of AVERAGES SMALL PADs

```
[34] Exit

"""

option = int(raw_input(menu_text))

if option == 1:

filename()

elif option == 2:

function2()

.

.

.

elif option == 34:

sys.exit()

else:

main_menu()
```

BIBLIOGRAPHY

BIBLIOGRAPHY

[1] W. Mittig, S. Beceiro-Novo, A. Fritsch, F. Abu-Nimeh, D. Bazin, T. Ahn, W.G. Lynch, F. Montes, A. Shore, D. Suzuki, N. Usher, J. Yurkon, J.J. Kolata, A. Howard, A.L. Roberts, X.D. Tang, and F.D. Becchetti. Active target detectors for studies with exotic beams: Present and next future. *Nuclear Instruments and Methods in Physics Research Section A: Accelerators, Spectrometers, Detectors and Associated Equipment*, 784:494 – 498, 2015. Symposium on Radiation Measurements and Applications 2014 (SORMA XV).

[2] D. Suzuki, M. Ford, D. Bazin, W. Mittig, W.G. Lynch, T. Ahn, S. Aune, E. Galyaev, A. Fritsch, J. Gilbert, F. Montes, A. Shore, J. Yurkon, J.J. Kolata, J. Browne, A. Howard, A.L. Roberts, and X.D. Tang. Prototype at-tpc: Toward a new generation active target time projection chamber for radioactive beam experiments. *Nuclear Instruments and Methods in Physics Research Section A: Accelerators, Spectrometers, Detectors and Associated Equipment*, 691:39 – 54, 2012.

[3] Joshua William Bradt. *MEASUREMENT OF ISOBARIC ANALOGUE RESONANCES OF* ^{47}Ar *WITH THE ACTIVE-TARGET TIME PROJECTION CHAMBER.* PhD thesis, Michigan State University, 2017.

[4] E.C. Pollacco, G.F. Grinyer, F. Abu-Nimeh, T. Ahn, S. Anvar, A. Arokiaraj, Y. Ayyad, H. Baba, M. Babo, P. Baron, D. Bazin, S. Beceiro-Novo, C. Belkhiria, M. Blaizot, B. Blank, J. Bradt, G. Cardella, L. Carpenter, S. Ceruti, E. De Filippo, E. Delagnes, S. De Luca, H. De Witte, F. Druillole, B. Duclos, F. Favela, A. Fritsch, J. Giovinazzo, C. Gueye, T. Isobe, P. Hellmuth, C. Huss, B. Lachacinski, A.T. Laffoley, G. Lebertre, L. Legeard, W.G. Lynch, T. Marchi, L. Martina, C. Maugeais, W. Mittig, L. Nalpas, E.V. Pagano, J. Pancin, O. Poleshchuk, J.L. Pedroza, J. Pibernat, S. Primault, R. Raabe, B. Raine, A. Rebii, M. Renaud, T. Roger, P. Roussel-Chomaz, P. Russotto, G. Sacc, F. Saillant, P. Sizun, D. Suzuki, J.A. Swartz, A. Tizon, N. Usher, G. Wittwer, and J.C. Yang. Get: A generic electronics system for tpcs and nuclear physics instrumentation. *Nuclear Instruments and Methods in Physics Research Section A: Accelerators, Spectrometers, Detectors and Associated Equipment*, 887:81 – 93, 2018.

[5] M. Hausmann, A.M. Aaron, A.M. Amthor, M. Avilov, L. Bandura, R. Bennett, G. Bollen, T. Borden, T.W. Burgess, S.S. Chouhan, V.B. Graves, W. Mittig, D.J. Morrissey, F. Pellemoine, M. Portillo, R.M. Ronningen, M. Schein, B.M. Sherrill, and A. Zeller. Design of the advanced rare isotope separator aris at frib. *Nuclear Instruments and Methods in Physics Research Section B: Beam Interactions with Materials and Atoms*, 317:349 – 353, 2013. XVIth International Conference on ElectroMagnetic Isotope Separators and Techniques Related to their Applications, December 27, 2012 at Matsue, Japan.

[6] J.J. Kolata, A.M. Howard, W. Mittig, T. Ahn, D. Bazin, F.D. Becchetti, S. Beceiro-Novo, Z. Chajecki, M. Febbrarro, A. Fritsch, W.G. Lynch, A. Roberts, A. Shore, and R.O. Torres-Isea. Fusion studies with low-intensity radioactive ion beams using an active-target time projection chamber. *Nuclear Instruments and Methods in Physics Research Section A: Accelerators, Spectrometers, Detectors and Associated Equipment*, 830:82 – 87, 2016.

[7] Yassid Ayyad, Wolfgang Mittig, Daniel Bazin, Saul Beceiro-Novo, and Marco Cortesi. Novel particle tracking algorithm based on the random sample consensus model for the active target time projection chamber (at-tpc). *Nuclear Instruments and Methods in Physics Research Section A: Accelerators, Spectrometers, Detectors and Associated Equipment*, 880:166 – 173, 2018.

[8] J. Bradt, D. Bazin, F. Abu-Nimeh, T. Ahn, Y. Ayyad, S. BeceiroNovo, L. Carpenter, M. Cortesi, M.P. Kuchera, W.G. Lynch, W. Mittig, S. Rost, N. Watwood, and J. Yurkon. Commissioning of the active-target time projection chamber. *Nuclear Instruments and Methods in Physics Research Section A: Accelerators, Spectrometers, Detectors and Associated Equipment*, 875:65 – 79, 2017.

[9] T. Ahn, D.W. Bardayan, D. Bazin, S. Beceiro Novo, F.D. Becchetti, J. Bradt, M. Brodeur, L. Carpenter, Z. Chajecki, M. Cortesi, A. Fritsch, M.R. Hall, O. Hall, L. Jensen, J.J. Kolata, W. Lynch, W. Mittig, P. OMalley, and D. Suzuki. The prototype active-target time-projection chamber used with twinsol radioactive-ion beams. *Nuclear Instruments and Methods in Physics Research Section B: Beam Interactions with Materials and Atoms*, 376:321 – 325, 2016. Proceedings of the XVIIth International Conference on Electromagnetic Isotope Separators and Related Topics (EMIS2015), Grand Rapids, MI, U.S.A., 11-15 May 2015.

[10] J. Bradt, Y. Ayyad, D. Bazin, W. Mittig, T. Ahn, S. Beceiro Novo, B.A. Brown, L. Carpenter, M. Cortesi, M.P. Kuchera, W.G. Lynch, S. Rost, N. Watwood, J. Yurkon, J. Barney, U. Datta, J. Estee, A. Gillibert, J. Manfredi, P. Morfouace, D. Prez-Loureiro, E. Pollacco, J. Sammut, and S. Sweany. Study of spectroscopic factors at n=29 using isobaric analogue resonances in inverse kinematics. *Physics Letters B*, 778:155 – 160, 2018.

[11] D. Bazin, J. Bradt, Y. Ayyad, W. Mittig, T. Ahn, S. Beceiro-Novo, L. Carpenter, M. Cortesi, A. Fritsch, J. J. Kolata, W. Lynch, and N. Watwood. The active target time projection chamber at nscl. *EPJ Web of Conferences*, 163, 11 2017.

[12] J. Giovinazzo, J. Pibernat, T. Goigoux, R. deOliveira, G.F. Grinyer, C. Huss, B. Mauss, J. Pancin, J.L. Pedroza, A. Rebii, T. Roger, P. Rosier, F. Saillant, and G. Wittwer. Metal-core pad-plane development for actartpc. *Nuclear Instruments and Methods in Physics Research Section A: Accelerators, Spectrometers, Detectors and Associated Equipment*, 892:114 – 121, 2018.

[13] Y. Giomataris, Ph. Rebourgeard, J.P. Robert, and G. Charpak. Micromegas: a high-granularity position-sensitive gaseous detector for high particle-flux environments. *Nuclear Instruments and Methods in Physics Research Section A: Accelerators, Spectrometers, Detectors and Associated Equipment*, 376(1):29 – 35, 1996.

[14] S. Beceiro-Novo, T. Ahn, D. Bazin, and W. Mittig. Active targets for the study of nuclei far from stability. *Progress in Particle and Nuclear Physics*, 84:124 – 165, 2015.

[15] Joshua William Bradt. MEASUREMENT OF ISOBARIC ANALOGUE RESONANCES OF 47Ar WITH THE ACTIVE-TARGET TIME PROJECTION CHAMBER, 2017.